Microporous and Mesoporous Materials 323 (2021) 111238

Contents lists available at ScienceDirect

Microporous and Mesoporous Materials

journal homepage: www.elsevier.com/locate/micromeso

Study of cancer cell cytotoxicity, internalization and modulation of growth factors induced by transferrin-conjugated formulations of metallodrug-functionalized mesoporous silica nanoparticles

Diana Díaz-García [a,b], Eva Fischer-Fodor [b,*], Cătălin Ioan Vlad [c,d], José M. Méndez-Arriaga [a], Sanjiv Prashar [a], Santiago Gómez-Ruiz [a,**]

[a] COMET-NANO Group, Departamento de Biología y Geología, Física y Química Inorgánica, E.S.C.E.T., Universidad Rey Juan Carlos, Calle Tulipán s/n, E-28933, Móstoles, Madrid, Spain
[b] Tumor Biology Department, The Institute of Oncology "Prof. Dr. I. Chiricuta", RO, 00015, Cluj-Napoca, Romania
[c] Department of Surgery, The Institute of Oncology "Prof. Dr. I. Chiricuta", RO, 400015, Cluj-Napoca, Romania
[d] Department of Surgery and Gynecological Oncology, University of Medicine and Pharmacy "Iuliu Hatieganu", RO, 400337, Cluj-Napoca, Romania

ARTICLE INFO

Keywords:
Mesoporous silica
Transferrin
Organotin
Titanocene
Cytotoxicity

ABSTRACT

Nano-sized materials have shown to have very high potential in anticancer therapy by an adequate tuning of their functionalization and physico-chemical properties. This study is focused on the synthesis and characterization of mesoporous silica nanoparticles (MSN) functionalized with a titanium(IV) or an organotin(IV) compound (therapeutic agents), fluorescein isothiocyanate (image agent) and transferrin (targeting molecule). The analysis of the biological activity of the metallodrug-functionalized systems with and without transferrin has been evaluated and the cell internalization with respect to the presence of the protein has been assessed. The biological results show, as expected, that Sn-based materials are more active than the Ti-based systems with some of the tin-functionalized nanoparticles being almost 50 times more active than carboplatin. In contrast, the cellular uptake seems to be higher in Ti-based materials, which take advantage of the stronger interaction with transferrin to internalize the cells with more effectivity. Finally, a study of vascular endothelial growth factor A (VEGF-A), human fibroblast growth factor 2 (FGF-2) and nuclear factor κβ transcription factor (NF-κβ) show that, specially the Sn-based MSNs, were able to modulate these factors in A2780 cells showing anti-angiogenic effects through VEGF-A and FGF-2, probably due to interaction of the materials with transferrin.

1. Introduction

Nanotechnology and nanomaterials have greatly advanced during the last 30 years because of their potential in many different fields of research [1]. In particular, in medicine and biomedicine, nanomaterials are still one of the main objects of study due to their exceptional properties. For example, silica-based nanostructured materials have been widely used in drug delivery due to the great adsorption capacity and the potential use of different functional groups on their surface, which give a high number of functionalization options to include a variety of therapeutic compounds of interest in medicinal chemistry [2]. The great versatility of silica-based nanostructured materials allows, not only the study of new therapies, but also diagnostic applications in different diseases. For example, silica-based theragnostic materials can easily be obtained by the simple incorporation of both a therapeutic agent and a fluorescent diagnosis fragment [3], and this kind of systems are currently being developed with special interest in the fight against cancer [4–6]. Considering the study of novel therapeutic approaches to treat cancer, almost 50 years ago, the discovery of cisplatin and its derivatives (carboplatin, oxaliplatin) and their anticancer properties (approved in the late 1960's by the Food and Drug Administration (FDA)) [7], were a revolution in the field of anticancer chemotherapy. Nevertheless, the wide variety of side effects as the major drawback of the use of platinum compounds, moved the research efforts to their replacement by new metallic complexes based on, for example, ruthenium, gold, iron, titanium and tin [8].

* Corresponding author.
** Corresponding author.
E-mail addresses: fischer.eva@iocn.ro (E. Fischer-Fodor), santiago.gomez@urjc.es (S. Gómez-Ruiz).

https://doi.org/10.1016/j.micromeso.2021.111238
Received 17 March 2021; Received in revised form 22 May 2021; Accepted 9 June 2021
Available online 12 June 2021

In the field of metal-based drugs against cancer, the use of transferrin as a potential formulation agent to influence the metallodrug-cell uptake has already been exploited by several groups [9]. Transferrin is a glycoprotein which acts as a specific carrier of iron in the blood because it is non-toxic and biodegradable, this protein is also being used as a cancer targeting agent, especially in those cell lines that have a greater number of transferrin receptors, with the aim of obtaining a greater accumulation of the therapeutic compound at the cellular level. In addition, it is well known that transferrin has a great ability to transport other metal ions in addition to iron [10], so this capacity can be exploited for therapeutic benefit. In this context, titanium compounds have shown good Ti-transferrin associations [11] and a high stability of this interaction which is based on the fact that transferrin can bind two Ti^{4+} ions [12]. Transferrin has therefore a multitude of potential therapeutic applications [13], such as iron sequestering in radiotherapy [14], delivery of therapeutic agents [15] and directly in cancer therapy promoting high cytotoxicity [16]. However, organotin(IV) derivatives, which are also being studied as an alternative to platinum complexes due to their potent cytotoxicity and lack of interaction with the Pgp glycoprotein reducing the promotion of multidrug resistance in cancer cells [17], have not been analysed in transferrin-mediated processes. Therefore, it is of interest to determine whether the use of transferrin might be a potential formulation alternative for metal-based therapeutic systems.

In the context of metal-based drugs with anticancer potential, our research group has already tested several metallodrugs supported on nanostructured silica-based systems [8,18–21]. These have proven to be cytotoxic against many cell lines, acting as non-classical drug-delivery systems, without the need of controlled release of the drug in order to be highly cytotoxic against the cancer cells with the system as a whole acting as antiproliferative agent [22]. In addition, the incorporation of a folate fragment in this kind of systems promoted better *in vitro* and *in vivo* activities against cancer [23–25].

Therefore, the idea of incorporating transferrin in silica-based materials functionalized with titanocene or organotin cytotoxic fragments emerged as an alternative to prepare novel nanoformulations with potential theragnostic properties by the incorporation of imaging agents, such as fluorescein isothiocyanate (FITC), which should give more insights into the mechanism of cellular action of these systems against transferrin-sensitive cell lines such as A2780. Thus, the aim of this study is the incorporation of transferrin in silica-based materials functionalized with metallodrugs in order to determine the potential impact of the use of transferrin as vector for the functionalized nanomaterials. In particular, we have chosen mesoporous silica nanoparticles (MSN) as supporting material due to their high surface area, which allows an adequate functionalization of several different fragments of biological interest, and a low particle size compatible with good performance as therapeutic agents.

2. Materials and methods

2.1. General remarks on the synthesis and characterization of the materials

All reactions were performed using standard Schlenk tube techniques in an inert atmosphere of dry nitrogen. Solvents were distilled from the appropriate drying agents and degassed before use. The reagents used in the preparation of the starting material MSN, namely, hexadecyltrimethylammonium bromide (CTAB) and tetraethyl orthosilicate (TEOS) were purchased from Acros Organics and Sigma Aldrich respectively. 3-Mercaptopropyltriethoxysilane (Fluorochem), trimethoxysilyl-propyldiethylenetriamine (Fluorochem), triphenyltin chloride (Sigma Aldrich), bis(cyclopentadienyl)titanium dichloride (Sigma Aldrich) and triethylamine (Acros Organics), were used for the preparation of the functionalized MSN based materials. The reagents for the carbodiimide-mediated coupling reactions, *N*-(3-dimethylaminopropyl)-N′-ethylcarbodiimide (EDAC), (*N*-morpholino) ethanesulfonic acid (MES), *N*-(3-dimethylaminopropyl)-N′-ethylcarbodiimide (EDAC), *N*-hydroxysuccinamide (NHS), hydroxylamine hydrochloride, fluorescein isothiocyanate (FITC) and transferrin human (Tf), were purchased from Sigma Aldrich. All reagents were used directly without further purification.

X-ray diffraction (XRD) pattern of the systems were obtained on a Philips Diffractometer model PW3040/00 X'Pert MPD/MRD at 45 kV and 40 mA, using a wavelength Cu Kα (λ = 1.5418 Å). Sn and Ti wt% determinations by X-ray fluorescence (XRF) were carried out with an X-ray fluorescence spectrophotometer Philips MagiX with an X-ray source of 1 kW and a Rh anode using a helium atmosphere. FT-IR spectra were prepared using KBr pellets with a spectrophotometer Termo Nicolet Avatar 380 FT-IR with a Michelson filter interferometer. Thermogravimmetry (TG) analyses were obtained with a Shimadzu mod. DSC-50Q operating between 30 and 800 °C (ramp 20 °C/min) at an intensity of 50 A in nitrogen. N_2 gas adsorption–desorption isotherms (BET) were performed using a Micromeritics ASAP 2020 porosimeter. DR UV–Vis measurements were carried out on a Varian Cary-500 spectrophotometer equipped with an integrating sphere and polytetrafluoroethylene (PTFE) as reference. ^{29}Si MAS NMR (^{29}Si magic angle spinning nuclear magnetic resonance) spectra, were recorded on a Varian-Infinity Plus Spectrometer at 400 MHz operating at 100.52 MHz proton frequency (4 μs 90° pulse, 4000 transients, spinning speed of 6 MHz, contact time 3 ms, pulse delay 1.5 s). Transmission electron microscopy (TEM) was carried out on a JEOL JEM 1010, operating at 100 kV. Scanning electron micrographs (SEM) and morphological analyses were carried out on a XL30 ESEM Philips with an energy-dispersive spectrometry system (EDS).

2.2. Synthesis of mesoporous silica nanoparticle (MSN)

The synthesis of the starting material MSN was carried out with a slight modification of the experimental procedure reported by Zhao et al. [26]. An aqueous solution of CTAB (1 g, 2.74 mmol) was prepared in 480 mL of Milli-Q water. Subsequently, sodium hydroxide (2 M, 3.5 mL) was added to the solution and the temperature increased to 80 °C. Afterwards, the silica precursor TEOS (5 mL, 22.4 mmol) was added dropwise under vigorous stirring and the mixture allowed to react for 2 additional hours. The resulting white precipitate was isolated by filtration and washed with abundant Milli-Q water and then with methanol and dried for 24 h at 80 °C in a stove. Finally, a calcination process at 500 °C was carried out for 24 h.

2.3. Functionalization with the different ligands

For the formation of MSN-MP, 2.0 g of the starting material (MSN) was dried at 80 °C under vacuum overnight. MSN was dispersed in 40 mL of dry toluene and 2.03 mL (8.40 mmol) of 3-mercaptopropyltriethoxysilane (MP) was added. The mixture was stirred at 110 °C for 24 h. Subsequently, the suspension was cooled to room temperature and centrifuged (6000 rpm, 10 min). The isolated solid was then washed with toluene and diethyl ether and dried overnight in a stove at 75 °C.

MSN-MP-DETATMS was synthesized from 1.2 g of MSN-MP, (previously dried at 80 °C under vacuum overnight), in 30 mL of dry toluene with 1.17 mL (6.48 mmol) of trimethoxysilyl-propyldiethylenetriamine (DETATMS) during 24 h at 110 °C (Scheme 1). The suspension was centrifuged, and the isolated solid was washed with toluene and diethyl ether and dried overnight in a stove (75 °C).

For the preparation of MSN-MP+DETATMS, 1.5 g of MSN was dried and dispersed in 30 mL of dry toluene. 1.52 mL (6.29 mmol) of MP and 1.46 mL (5.66 mmol) of DETATMS were added at the same time (Scheme 2). The mixture was kept under stirring for 24 h at 110 °C. The suspension was centrifuged, washed and dried in the same manner as the other materials.

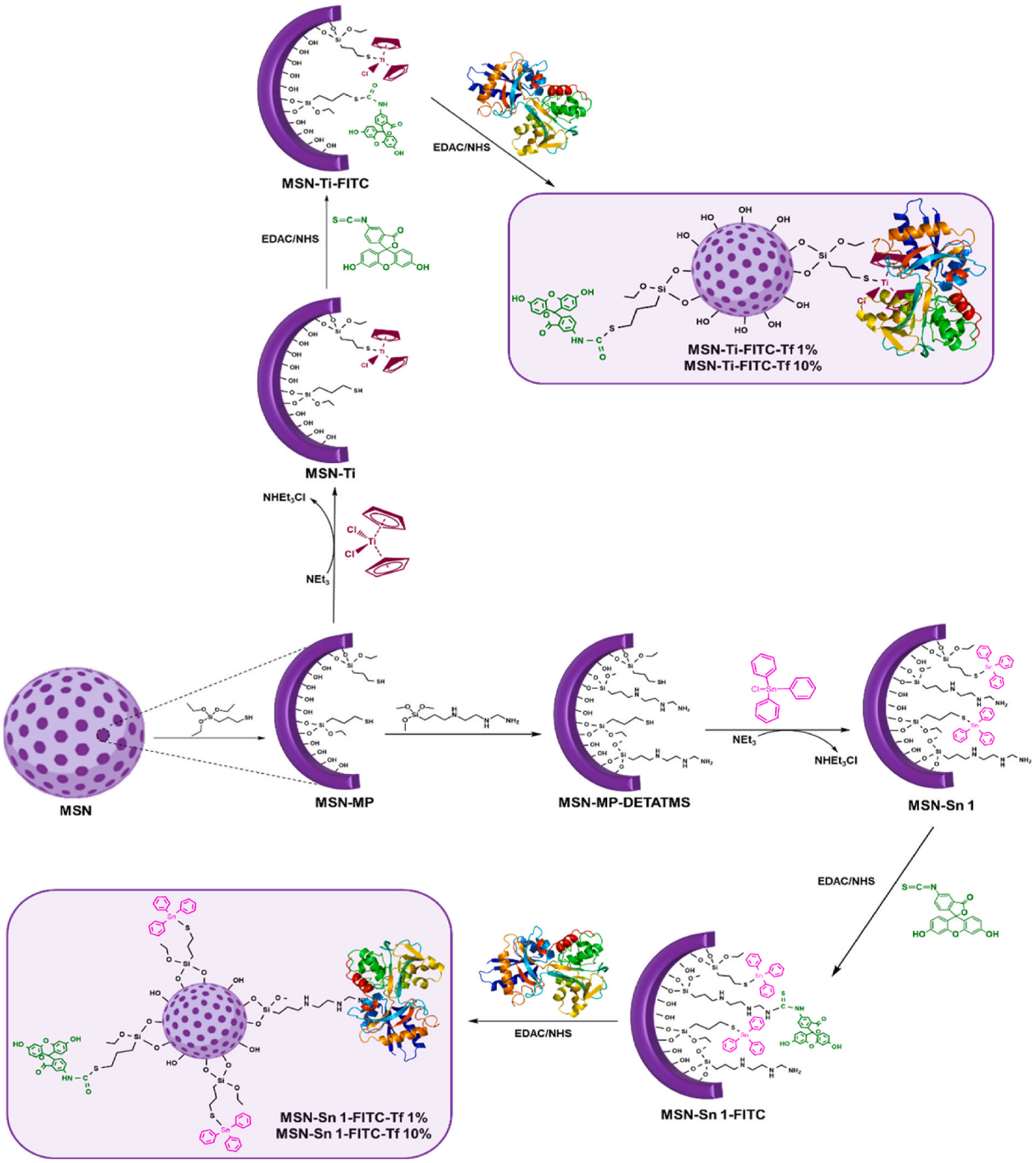

Scheme 1. Synthesis of the materials of tin series 1 and titanium series.

2.4. Functionalization with organometallic compounds

The synthesis of MSN-Sn1 was carried out as follows: 1.2 g of MSN-MP-DETATMS and 74.9 mg of $SnPh_3Cl$ (0.19 mmol, considering that MSN-MP-DETATMS has a 0.519 % wt. of S, this corresponds to a 1:1 ratio Sn:S) were dispersed in 30 mL of dry toluene and 54.15 μL of NEt_3 (0.39 mmol) (Scheme 1). The suspension was stirred 24 h at 110 °C. Subsequently, the mixture was centrifuged, the resulting solid washed with toluene and ethanol and dried overnight in a stove (75 °C). For MSN-Sn2, 1.5 g of MSN-MP+DETATMS, 166.3 mg of $SnPh_3Cl$ (0.43 mmol, MSN-MP+DETATMS has a 0.922% of S) and 120.15 μL of NEt_3 (0.86 mmol) were used and the same procedure was followed as for MSN-Sn1 (Scheme 2).

For the formation of MSN-Ti, 0.85 g of MSN-MP and 18 mg of $TiCp_2Cl_2$ ($Cp = \eta^5\text{-}C_5H_5$) (0.07 mmol, considering that MSN-MP has a 0.407 % wt. S, this correspond to a 1:1 ratio Ti:S) were dispersed in 30 mL of dry toluene and 20.2 μL NEt_3 (0.014 mmol) (Scheme 1). The mixture was stirred for 24 h at 110 °C.

2.5. Incorporation of imaging and targeting agents

For the functionalization of the materials with FITC (imaging agent), an EDAC-mediated coupling reaction was carried out (Schemes 1 and 2). 50 mg of FITC (0.13 mmol, 5% functionalization of each material) was dissolved in 12.5 mL of DMSO in an ultrasonic bath, and this solution was added to 100 mL of MES buffer solution containing 40 mg (0.21 mmol) of EDAC and 60 mg (0.52 mmol) of NHS. The mixture was stirred for 15 min at room temperature. Subsequently, 1.0 g of functionalized-

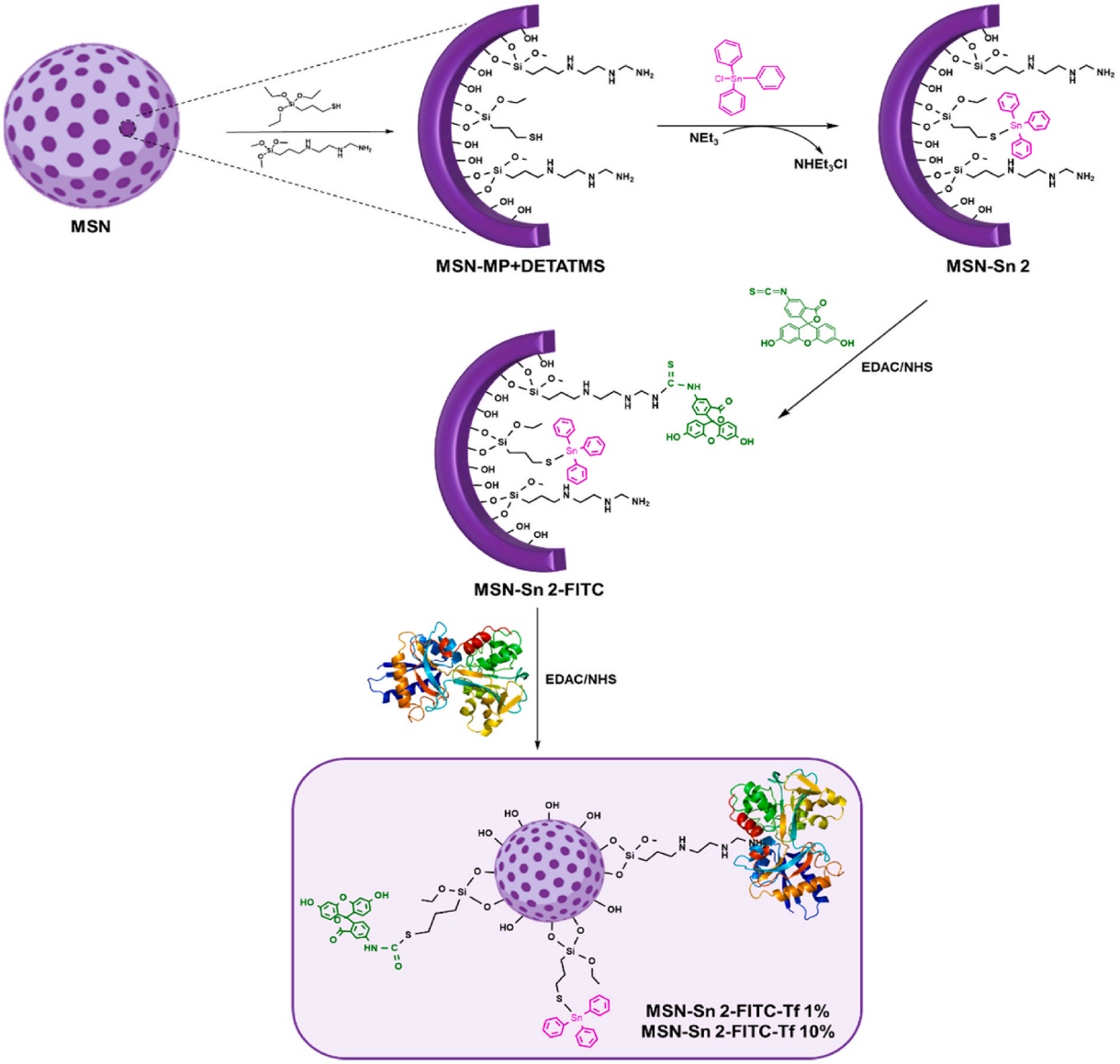

Scheme 2. Synthesis of the materials of tin series 2.

MSN was added to the EDAC solution, the resulting mixture was left for 2 additional hours at room temperature under vigorous stirring. Finally, 86 mg (1.24 mmol) of hydroxylamine was added to the mixture in order to quench the reaction. The mixture was centrifuged, washed with DMSO, Milli-Q water and ethanol in order to remove the excess of reagents, and dried overnight in a stove (75 °C). The products obtained using this method were MSN-Sn 1-FITC, MSN-Sn 2-FITC, MSN-Ti-FITC.

The incorporation of transferrin was carried out using a modification of an EDAC-mediated coupling reaction (Schemes 1 and 2). 0.8 mg or 8 mg of Tf (1 or 10% functionalization in mass with respect to FITC materials) was dissolved in 40 mL of PBS. A solution of EDAC and NHS (20 or 200 μL of 1 mg/mL) added and the mixture stirred for 45 min at room temperature. Subsequently, 80 mg of MSN-Sn 1-FITC, MSN-Sn 2-FITC or MSN-Ti-FITC was added, and the mixture stirred for 2 additional hours at room temperature. The mixture was then centrifuged and the solid product dried under vacuum at room temperature, overnight. Using this method, the following materials MSN-Sn 1-FITC-Tf 1%, MSN-Sn 2-FITC-Tf 1%, MSN-Ti-FITC-Tf 1%, MSN-Sn 1-FITC-Tf 10%, MSN-Sn 2-FITC-Tf 10%, MSN-Ti-FITC-Tf 10% (Table 1) were prepared.

Table 1
Different series of functionalized materials synthesized in this study.

Tin Series 1	Tin Series 2	Titanium Series
MSN-MP-DETATMS	MSN-MP DETATMS	MSN-MP
MSN-Sn 1	MSN-Sn 2	MSN-Ti
MSN-Sn 1-FITC	MSN-Sn 2-FITC	MSN-Ti-FITC
MSN-Sn 1-FITC-Tf 1%	MSN-Sn 2-FITC-Tf 1%	MSN-Ti-FITC-Tf 1%
MSN-Sn 1-FITC-Tf 10%	MSN-Sn 2-FITC-Tf 10%	MSN-Ti-FITC-Tf 10%

2.6. General remarks on cell culture and biological assays

The *in vitro* testing was performed on A2780 human ovarian carcinoma cell line acquired from the European Collection of Authenticated Cell Cultures ECACC (Salisbury, UK) cultivated in RPMI-1640 cell culture media, supplemented with 10% fetal calf serum and penicillin with streptomycin (all from Sigma Aldrich Chemie GmbH, Taufkirchen, Germany). Cells were incubated under a humidified atmosphere containing 5% CO_2 at 37 °C. The serial dilutions of each compound were prepared from 10 mg/mL to 0.078 mg/mL using Phosphate Buffered Saline solution (PBS, from Sigma Aldrich) as a diluent.

2.7. Cytotoxicity tests

For the viability testing, the cells were cultivated on 96-well plates, at a concentration of 4×10^4 cells/mL in 190 μL media in each well. All compounds were diluted in absolute ethanol to obtain a 10 mg/mL stock solution and starting from this concentration, seven serial dilutions were prepared in phosphate buffered saline solution (PBS, from Sigma Aldrich). The serial dilutions were used to treat the individual wells containing A2780 cells, in duplicates. The MTT colorimetric viability test was performed, following a method applied earlier to assess nanostructures on A2780 ovarian cells [22]. The dispersed materials replaced a proportion of 1/20 of the cell culture media (10 μL added to each well); the final concentration of the materials in the cell suspension were between 3.9 and 500 μg/mL. Untreated cells were used as reference values, the wells filled with cell culture media only as blank, and the colour controls were the wells without cells, or wells with media and FITC for the materials functionalized with that compound, respectively. After 24 h of incubation at 37 °C, the cell culture media was removed, and the wells were treated for 1 h with 100 μL (1 mg/mL solution) of 3-(4,5-dimethylthiazol-2-yl)-2, 5-diphenyltetrazolium bromide (MTT) dye in Hank's media (both from Sigma Aldrich Chemie GmbH, Taufkirchen, Germany). The MTT solution was then removed and 150 μL of DMSO was added to solubilize the purple formazan crystals formed inside the living cells, which are able to metabolize MTT. The plates were subjected to colorimetric measurements at 570 nm, using a Synergy 2 multiplate reader (from BioTek Company, Winooski, VT, USA). The experiments were repeated three times. The absorption data were analysed with the GraphPad Prism 5 software (from GraphPad Software, La Jolla, CA, USA) and the half maximal inhibitory concentrations (IC_{50}) were calculated from the non-linear regression curves, in the 95% confidence interval.

2.7.1. ELISA tests

For quantitative measurements on certain proteins implicated in the cell death mechanisms, the chosen method was the enzyme-linked immunosorbent assay (ELISA). For this purpose, the A2780 cells were seeded on 6-well plates, at a density of 6×10^5 cells in 2850 μL media per well. After 24 h, when almost all the cell population was attached and the cells were in exponential growth phase, the wells were treated with 150 μL diluted material (2 wells for each MSN-based material), to obtain a final concentration corresponding to IC_{50} for each compound. As reference, untreated cells were used; in this case 150 μL PBS was dispensed onto the cells. The cells were subjected to the treatments for 24 h, subsequently the media from the wells was removed and centrifuged at 4000 rpm for 20 min. The supernatants were harvested, their total protein content was measured using the Bradford method. The samples concentration was normalized by diluting with the dilution buffer from the ELISA kit, subsequently aliquoted and freezed at −80 °C. In the meantime, the wells having A2780 cells still attached on their surface were carefully rinsed twice with PBS, and then 500 μL cold cell extraction buffer (component of the NF-κβ phosphorilated p65 ELISA kit, described below) was added to each well. The plates were kept on ice for 20 min, and afterwards the buffer was collected, centrifuged and the protein content of each sample was measured using the Bradford method, as described earlier [27]. Cell lysates were stored at −80 °C before the final testing.

The Vascular Endothelial Growth Factor A (VEGF-A) was measured in the cell culture supernatants after 48 h exposure. The protocol was carried out according to the manufacturer's indications (Human VEGF PicoKine ELISA Kit, from BosterBio, Pleasanton, CA, USA). 100 μL of each diluted sample of cell culture supernatants, in duplicate, and 100 μL of human VEGF standard solutions was added to the precoated 96-well plates and incubated at 37 °C for 90 min. The plate content was discarded and 0.1 mL of biotinylated anti-human VEGF antibody working solution was added into each well. The sealed plate was incubated at 37 °C for 1 h. The plate was washed with PBS three times, 100 μL of prepared Avidin-Biotin-Peroxidase Complex (ABC) working solution was added into each well and the seal plate was incubated again at 37 °C for 30 min. After that time, the plate was washed 5 times with PBS, 90 μL of prepared 3,3′,5,5′-tetramethylbenzidine (TMB) colour developing agent was added into the wells and incubated at 37 °C for 25 min in dark. 100 μL of prepared TMB stop solution was then added into each well. The 96-well plate was read at 450 nm on TECAN Sunrise ELISA plate reader with Magellan software (Tecan Group, Männedorf, Switzerland).

The Human Fibroblast Growth Factor 2 (FGF-2) was measured in the cell culture supernatants after 48 h exposure. The protocol was carried out according to the manufacturer's indications (Human FGF-Basic Colorimetric OmniKine ELISA KIT, from Assay Biotechnology, Fremont, CA, USA). 100 μL of each diluted sample of cell culture supernatants, in duplicate, and 100 μL of human FGF standard solutions was added to the precoated 96-well plates and incubated at 37 °C for 90 min. The liquid was removed from the wells and subsequently washed 4 times with a wash buffer. 100 μL of Dilute Biotinylated Detection Antibody and the 96-well plate was incubated at 37 °C for 90 min. After that time, the plate was washed 4 times. 100 μL of Streptavidin-HRP was added into each well and incubated at room temperature for 30 min. The plate was washed 4 times. 100 μL of Ready-to-Use Substrate was added into each well and incubated at room temperature for 15 min. Finally, 100 μL of Stop Solution was added and the 96-well plates was read at 450 nm on TECAN Sunrise ELISA plate reader.

The nuclear factor κβ transcription factor (NF-κβ) phosphorylated p65 (pS536) isoform was measured semi-quantitatively using a SimpleStep Elisa kit from Abcam, Cambridge, United Kingdom. On the precoated strip wells 50 μL the thawed, centrifuged lysate samples were dispensed, and serial dilutions of the standard lyophilized control (provided by the kit) were added in duplicates. Subsequently, 50 μL antibody cocktail (caption and detector antibody mix) was added to each well, the plates were sealed, incubated for 1 h on an orbital shaker (ES-20 from Biosan, Riga, Latvia) and then washed three times with automated washer, using a buffer, component of the kit. The wells were subsequently filled with 100 μL TMB substrate solution and incubated for 15 min in the dark, while shaking. Finally, 100 μL stop solution was added to each well, and the plate was read at 450/540 nm using the above-mentioned Elisa reader. The Magellan software provided a calibration curve and calculated the individual phosphorylated NF-κβ concentrations in the samples as percentages of the quantity of the lyophilized standard NF-κβ protein normalized according to their protein content.

2.7.2. Cellular uptake assay

The cellular uptake of all FITC-MSN materials was studied by fluorescence assay. For that, 950 μL of suspension with 7×10^5 cell were incubated at 37 °C in Falcon tubes, with 50 μL (5 mg/mL) of each FITC material at different exposure times (15 min, 30 min, 1 h, 2 h and 4 h). After the necessary time, the suspensions were centrifuged, the pellets were washed two times with 500 μL of cold PBS and 100 μL of pellet suspension was added to a 96-well plate. The plates were read at sensitivity 70, with excitation at 485 nm and emission at 528 nm, using a Synergy 2 multi-plate reader (from BioTek Company, Winooski, VT, USA).

2.7.3. The electrokinetic Z-potential measurement

Z-potential measurements were carried out on a ZetaView Particle metrix at pH 7.0. Biostatistical analysis was performed using the GraphPad Prism 5 software (GraphPad Software, La Jolla, CA, USA) and Principal Component Analysis was completed with StatSoft Statistica 12 software (Stat-Soft Inc. Tulsa, OK, USA).

2.7.4. Stability studies

Tin release of the materials MSN-Sn 2-FITC and MSN-Sn 2-FITC-Tf 10% was carried out in order to analyze the stability of the metal in the silica system. For this, 5 mg of the materials was dispersed in 5 mL of simulated body fluid (pH 7.4 PBS buffer) and incubated at 37 °C with slight shaking (30 rpm) using a Roto-587 Therm incubator (Benchmark) for 3, 8, 24, 48 and 72 h. After that time, the suspensions were

centrifuged (1000 rpm, 10 min) and filtered through a nylon filter (0.2 μm) by ICP-AES, using a Varian Vista AX Pro (λ_{Sn} = 283.998 nm).

For the analysis of transferrin release, all the Tf-containing materials were incubated under the same conditions (37 °C and pH 7.4) at concentrations of 5 mg/mL for 15, 30, 60, 120 and 240 min (the same time periods as the cellular uptake assays). The suspensions were centrifuged (1000 rpm, 10 min) and the absorbance measurements were monitored using a spectrophotometer (SP-830) at 218 nm (absorption maximum of transferrin in PBS).

CD spectra were recorded on a JASCO J-815 spectrometer at 37 °C, with a scanning speed of 20 nm/min in a 200–260 nm range, using 5 mm glass cuvettes. The samples were solved/suspended in PBS buffer (pH 7.4).

3. Results and discussion

3.1. Synthesis and characterization of co-functionalized nanomaterials

3.1.1. Synthesis of the materials

The initial mesoporous silica nanoparticles (MSN) were first functionalized via grafting reactions with two ligands, MP and DETATMS, by two different synthetic protocols. Firstly, the preparation of MSN-MP-DETATMS which was achieved by the functionalization with the MP ligand (1:1 mass ratio MSN:MP) and, subsequently, the reaction with DETATMS ligand (1:1 mass ratio MSN-MP:DETATMS) for 24 additional hours. The second method consists of a one pot grafting reaction of both ligands (1:1:1 mass ratio MSN:MP:DETATMS) during 24 h.

The materials obtained (MSN-MP-DETATMS and MSN-MP+DETATMS) were then further functionalized with a tin compound ($SnPh_3Cl$) in the presence of triethylamine to achieve the formation of the supported tin(IV) thiolate materials (MSN-Sn 1 and MSN-Sn 2) similar to those that have previously demonstrated promising cytotoxic activity in recent studies carried out by our research group [22–25]. Additionally, the titanocene derivative ($TiCp_2Cl_2$) was grafted onto MSN-MP in the presence of triethylamine to give the material MSN-Ti, following a similar method to that described by us in a previous study with SBA-15 as support [21].

A subsequent coupling reaction catalysed by EDAC was carried out to incorporate FITC as imaging agent and transferrin (Tf) as the targeting formulating macromolecule. In all cases, a functionalization with 1 or 10% of Tf was studied in order to determine the potential effect of the incorporation of this protein in the final biological properties of the systems. Using this method, the following materials were obtained: MSN-Sn 1-FITC, MSN-Sn 2-FITC, MSN-Ti-FITC, MSN-Sn 1-FITC-Tf 1%, MSN-Sn 2-FITC-Tf 1%, MSN-Ti-FITC-Tf 1%, MSN-Sn 1-FITC-Tf 10%, MSN-Sn 2-FITC-Tf 10%, MSN-Ti-FITC-Tf 10%.

To study in more detail the conjugation reaction of transferrin and the nanostructured materials, the potential amount of transferrin covalently bound to the silica nanoparticles was determined by monitoring the reaction by UV–visible spectroscopy. The reduction of intensity of the transferrin peaks in the solution, after the coupling reaction with EDAC and filtering of the silica-based system, of around 20% with respect to the starting amount of transferrin (for both the 1% and 10% Tf loading) was observed (see for example Figure S1 of supplementary material). However, for the conjugation efficiency, one cannot rule out that the other 80% of transferrin that is not covalently bound to the silica-based system, may not actively involved in the biological processes (of cell internalization, for example) because potential adsorption processes, which are very usual considering both the size of the protein and the size of the nanoparticles, may also play an important role in all the biological tests.

All the nanomaterials were characterized by diverse instrumental techniques in order to determine the main structural and compositional features of the synthesized systems. It is important to note that in the case of the loading with the cytotoxic and imaging agent the functionalization seems to be achieved mainly inside the pore of the mesoporous system (see section 3.1.4). However, the incorporation of transferrin in the last synthetic step is only possible through the reaction with the corresponding fragments (titanocene or polyamine compound), which are also, in a very low quantity, located on the external surface of the nanoparticles. This is due to the size of transferrin which is higher than the size of the pores of the MSNs, Tf is an oblate spheroid of ca. 4.6 × 4.6 × 1.6 nm, while the pore size of the MSNs is ca. 2.3 nm.

3.1.2. Powder X-ray diffraction and fluorescence studies

All the synthesized materials were analysed by low angle powder XRD. They all present the typical peaks which correspond to a hexagonally ordered silica (Fig. 1). The starting MSN showed three main peaks associated with the 100, 110 and 200 Miller planes at 2θ of 2.53, 4.32 and 4.98°, respectively. The intensity of these peaks (specially of those of the planes 110 and 200) decreased drastically after the functionalization with the ligands and even more with the subsequent incorporation of tin or titanium and FITC. After introducing transferrin, the diffractograms obtained had the same pattern, although the intensity of the peaks was very low because all the incorporated molecules seem to be blocking the dispersion centres of the MSN material and thus reducing the diffraction intensity of the porous system. This effect is more pronounced in the case of the functionalization with transferrin at 10% which seems to completely cover the surface of the nanoparticles limiting their diffracting ability.

It is important to note that the decrease in the intensity of the signals for the materials with both ligands MP and DETATMS (MSN-MP+DETATMS in Fig. 1 left and MSN-MP-DETATMS in Figure S2) is much higher than that found for the MSN-MP material (Fig. 1 right). Table 2 shows the data of the peaks for each material. One can observe that both the position of the peak associated with the *hkl* 100 plane and the crystallite size (a_0) are, as expected, very similar in all materials and it can be deduced that the functionalization reactions do not cause a significant change.

The quantification of sulphur, tin and titanium was performed by X-ray fluorescence (Table 3). The analysis of the amount of S in the materials showed that MSN-MP+DETATMS has a higher % S wt. (ca. 0.92%) than its analogue MSN-MP-DETATMS (ca. 0.52 % wt. S). This difference in the amount of S can be explained by the fact that not all the MP ligand is covalently attached to the material (Scheme S1 of Supplementary Material). This is corroborated by the % wt. S in MSN-Sn 2-FITC, that significantly decreases to ca. 0.40 % wt. S (even including the incorporation of FITC that contains S in its structure), suggesting that some of the MP in MSN-MP+DETATMS is adsorbed in the material and is eliminated after the successive washing steps of the reaction. The incorporation of FITC increases the quantity of S in the material MSN-Sn 1-FITC to ca. 0.72 % wt. S from its parent system MSN-MP-DETATMS (ca. 0.52 % wt. S). Interestingly, in MSN-Ti-FITC, the % wt. S is very large and suggests that both covalent incorporation and adsorption of FITC takes place.

The analysis of the amount of tin in the systems showed that MSN-Sn 1-FITC has ca. 4.5% wt. Sn. However, its analogue MSN-Sn 2-FITC contains only ca. 0.5 % wt. Sn. This is probably due to the fact that the $SnPh_3Cl$ functionalization in MSN-Sn 1-FITC is from the reaction of MSN-MP-DETAMTS material, which has a higher amount of covalently attached MP ligand compared to MSN-MP+DETATMS, which is used for the preparation of MSN-Sn 2-FITC. In this context, a significant amount of $SnPh_3$ moieties may also be directly bound to the silanol groups of MSN in MSN-Sn 1-FITC.

3.1.3. Thermogravimmetric analysis

The quantification of the MP and DETATMS ligands was carried out by thermogravimmetry quantifying the weight loss between 120 and 650 °C (Fig. 2). The incorporation of MP and DETATMS is approximately the same for both synthetic methods and is ca. 18 % wt (Table 3). This is comparable with other ligands, such as aminopropyl systems or similar, functionalized in other silica-based systems [24].

3.1.4. Nitrogen adsorption-desorption isotherms

Selected materials were also characterized by nitrogen adsorption-

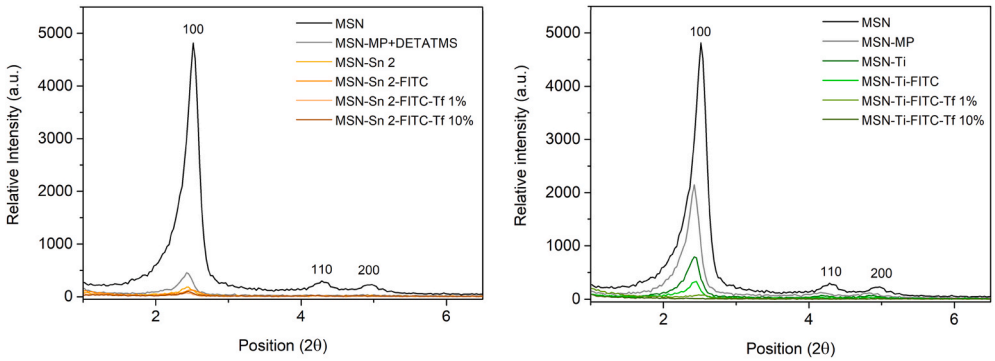

Fig. 1. XRD patterns of all the materials of Sn 2 series (left) and titanium series (right).

Table 2
XRD data for all the MSN materials.

	Material	(*hkl*)	2θ (°)	d_{hkl} (Å)	a_0 (Å)
	MSN	100	2.53	34.91	40.31
		110	4.32	20.44	–
		200	4.98	17.75	–
Tin Series 1	MSN-MP-DETATMS	100	2.49	35.46	40.95
	MSN-Sn 1	100	2.46	35.89	41.44
	MSN-Sn 1-FITC	100	2.46	35.94	41.51
	MSN-Sn 1-FITC-Tf 1%	100	2.39	36.93	42.64
	MSN-Sn 1-FITC-Tf 10%	100	–	–	–
Tin Series 2	MSN-MP+DETATMS	100	2.45	36.09	41.68
	MSN-Sn 2	100	2.42	36.48	42.13
	MSN-Sn 2-FITC	100	2.48	35.53	41.03
	MSN-Sn 2-FITC-Tf 1%	100	2.43	36.32	41.94
	MSN-Sn 2-FITC-Tf 10%	100	2.46	35.92	41.48
Titanium Series	MSN-MP	100	2.43	36.38	42.01
	MSN-Ti	100	2.43	36.32	41.94
	MSN-Ti-FITC	100	2.44	36.24	41.85
	MSN-Ti-FITC-Tf 1%	100	2.55	35.59	41.10
	MSN-Ti-FITC-Tf 10%	100	–	–	–

Table 3
Quantification of S and metals by XRF and ligands by TG.

Material	% S[a]	% Sn[a]	% Ti[a]	% MP and DETATMS[b]
MSN-MP	0.407	–	–	n.a.
MSN-MP-DETATMS	0.519	–	–	17.98
MSN-MP+DETATMS	0.922	–	–	18.02
MSN-Sn 1-FITC	0.762	4.47	–	17.98
MSN-Sn 2-FITC	0.396	0.483	–	18.02
MSN-Ti-FITC	2.9	–	0.453	–

[a] Determined by XRF.
[b] Determined by TG; n. a: not analysed.

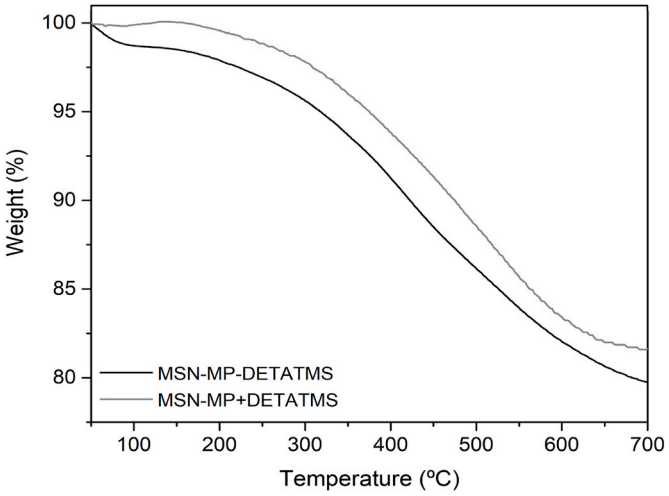

Fig. 2. TG analysis of the functionalized materials with the ligand MP and DETATMS by the two synthetic methods.

desorption (BET) to determine some of their textural features (Fig. 3, Table 4 and Figures S3 and S4 of supplementary material). As expected, the starting material MSN has a large surface area (ca. 900 m^2/g) and pore volume (0.64 cm^3/g), which decrease after the incorporation of the compounds of interest (MP and DETATMS, Sn or Ti compound and Tf). For example, a dramatic decrease of the surface area was observed for MSN-Sn 1-FITC-Tf 10% (ca. 18 m^2/g) or MSN-Ti-FITC- Tf 10% (140 m^2/g). As expected, the intermediate materials, namely, MSN-Sn 1-FITC (ca. 54 m^2/g) or MSN-Ti-FITC-Tf 10% (739 m^2/g) have surface areas higher than MSN-Sn 1-FITC-Tf 10% or MSN-Ti-FITC-Tf 10% but lower than MSN. The large decrease in the surface area of MSN-Sn 1-FITC-Tf 10% or MSN-Ti-FITC-Tf 10% with respect to their parent material, confirms the incorporation of the protein in the system.

The isotherms of MSN, MSN-Ti-FITC and MSN-Ti-FITC-Tf 10% are type IV isotherms (considering the IUPAC classification [28]) due to typical multilayer adsorption of porous materials with a hysteresis cycle characterized by irregular condensation of the capillaries, similar to other systems based on mesoporous functionalized-organosilica nanoparticles [29]. However, in the case of MSN-Sn 1-FITC and MSN-Sn 1-FITC-Tf 10% the isotherms showed a relatively low adsorption of nitrogen leading to isotherms which are closer to type III (typical of non-porous materials or materials with low porosity) but with a hysteresis loop, as previously reported in other similar systems based on silica [23] or titania nanoparticles [30].

The pore size distribution of MSN (Figure S5 and S6 of supplementary material) is narrow and centred in 2.87 nm, as expected for a mesoporous material. The pore size decreases after the functionalization with the metal compounds, for example, with titanium complex and FITC in MSN-Ti-FITC, the diameter is ca. 2.1 nm, while in all the other cases the pore size is < 2.0 nm (Figure S6), which are the lower measurement limits of the porosimeter. The decrease in the pore size indicates that most of the functionalization with the different agents has taken place inside the pores of the system. This is also observed in the pore volume change of the systems. The MSN starting material has a pore volume of 0.64 cm^3/g, and after the different functionalizations, for example for the final material MSN-Sn 1-FITC-Tf 10%, the volume decreases more than 21 times (V_p = 0.03 cm^3/g), while for the material MSN-Ti-FITC-Tf 10% the pore volume decreases almost 4 times (Vp = 0.17 cm^3/g), showing the lower pore saturation of the materials of the titanium series. As explained in section 3.1.1. the functionalization of the cytotoxic fragments and the imaging agent occurs mainly inside the pore of the mesoporous system, however, the incorporation of transferrin is only possible through the reaction with the agents located in the external surface of the nanoparticles due to the size of the protein which is greater than the size of the pores of the MSNs.

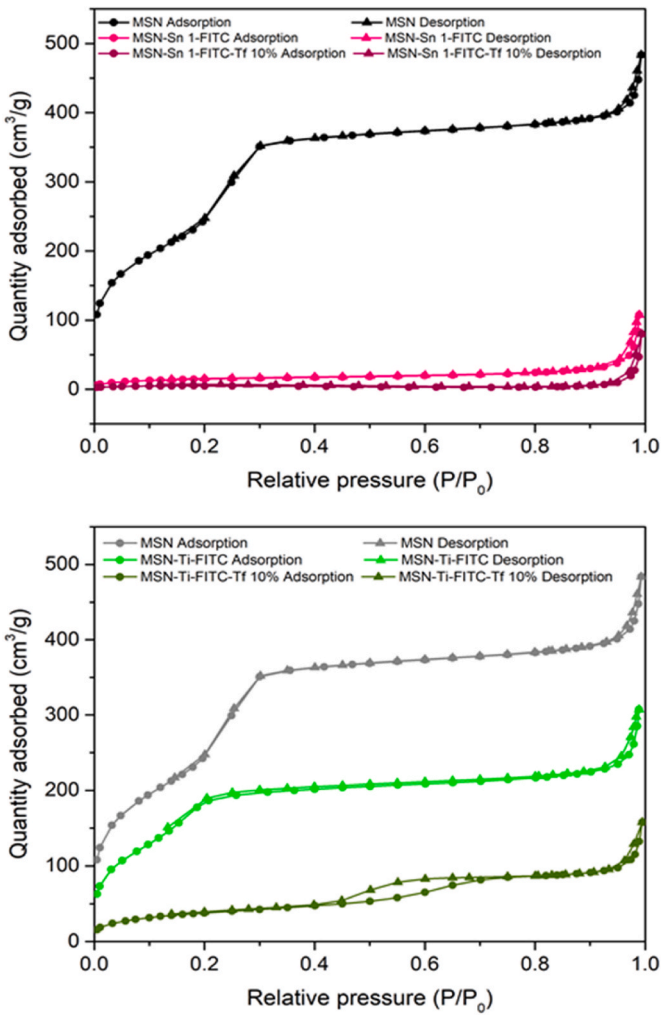

Fig. 3. Nitrogen adsorption–desorption isotherms of materials of Sn 1 series (up) and titanium series (down).

Table 4
Textural parameters of selected MSN-materials obtained by nitrogen adsorption–desorption analysis.

Material	BET Surface (m^2/g)	Pore Volume (cm^3/g)	Pore Diameter (nm)
MSN	892	0.64	2.87
MSN-MP	617	0.54	2.51
MSN-MP-DETATMS	251	0.14	2.18
MSN-Sn 1-FITC	54	0.08	<2.0
MSN-Sn 1-FITC-Tf 10%	18	0.03	<2.0
MSN-Ti-FITC	739	0.38	2.07
MSN-Ti-FITC-Tf 10%	140	0.17	<2.0

3.1.5. FT-IR studies

The IR spectra of the different functionalized systems show the typical bands associated with silica nanoparticles. Thus, one can observe, firstly, a band at 3400 cm^{-1} that together with the band at 1650 cm^{-1}, correspond to the vibration of the silanol groups (Si–OH), secondly, twin characteristic bands at 1100 cm^{-1} and 450 cm^{-1} which are due to the vibration of Si–O–Si bonds and thirdly a band at 800 cm^{-1} which is associated with the deformation of Si–OH bonds. In addition, in the functionalized systems significant bands (Fig. 4), are situated at ca. 2850 cm^{-1}, associated with the C–H bonds of alkanes and *N*–H of amines, and at 1450 cm^{-1}, due to the C═C bonds, confirming the functionalization of the silica nanoparticles with the different ligands. The functionalization of Tf and FITC through an EDAC coupling can be deduced by the appearance of small peaks at ca. 1700 cm^{-1} associated to amide C═O stretching vibrations, and the peaks at 1220 cm^{-1} and 700 cm^{-1} corresponding to amide *N*–H deformation and C–N stretching vibrations, as observed previously in other metallodrug functionalizations through the formation of amido bonds [31]. These peaks are more defined for the final materials MSN-Sn 2-FITC-Tf 1% and MSN-Sn 2-FITC-Tf 10% (Fig. 4, right) because MSN-Sn 2-FITC-Tf 1% and MSN-Sn 2-FITC-Tf 10% have more amide bonds especially due to the incorporation of Tf [32].

3.1.6. UV–visible measurements

The materials were also characterized by DR UV–Vis spectroscopy to determine the incorporation of the different agents in the MSN-materials. It has previously been observed that this method can help to confirm the incorporation of different ligands or metal complexes in the nanostructured silica [31,33,34]. Fig. 5 shows the DR UV–Vis spectra of the studied materials. In all of them a signal at ca. 200–205 nm, corresponding to both MP and DETATMS ligands, was observed and is in agreement to that observed in other analogous materials with similar ligands in the silica. In addition, the incorporation of FITC compound was confirmed by the appearance of two bands at ca. 240 and 495 nm in all the spectra. Interestingly, the spectra of the titanium series (Fig. 5A) show two bands around 240 and 290 nm associated with the known interactions of Ti with Tf [35], in which two equivalents of Ti(IV) usually bind to transferrin. In the Sn series, a peak at ca. 320 nm appears together with an increase in the intensity of the FITC peak at around 500 nm, which is presumably due to the interaction of Tf with both the $SnPh_3$ moiety and the FITC. This indicates clear differences in the mode of interaction M-Tf between Sn and Ti, and a higher affinity in the formation of the Ti-Tf bond compared with the Sn-Tf bond.

3.1.7. Solid-state ^{29}Si NMR spectroscopy

The Sn 2 series of materials was characterized by ^{29}Si MAS NMR. The spectra of MSN, MSN-MP+DETATMS, MSN-Sn 2, MSN-Sn 2-FITC-Tf 1% (Fig. 6) confirmed the signals associated with Q^2, Q^3 and Q^4 peaks (between ca. −135 and −90 ppm), which are clearly seen in all the studied materials. Interestingly the intensity of the Q peaks associated with the unmodified MSN is very high (the highest of all materials of the series), however, after incorporation of the different fragments (MP, DETATMS, Sn compound, FITC and Tf) the intensity of the Q peaks decreased and two additional peaks of either low or medium intensity were also observed in the spectra (T^2 and T^3, at ca. −61 ppm and −69 ppm) and are associated with the formation of the Si–O–Si bonds ($(SiO)_2SiOH$–R) and ($(SiO)_3Si$–R). All these results are in agreement with those observed previously by our and other groups in functionalization reactions similar to those described here [36-38].

3.1.8. Z-potential measurements

One of the most interesting properties in the biological therapeutic study of nanostructured materials is the charge of the systems and their hydrodynamic size to observe if the nanostructured materials have potential to be applied in physiologic medium. The charge of nanoparticles is usually affected by the different modifications and in this case the incorporation of the different agents caused several changes in the charge of the systems (Table 5). In particular, the incorporation of the MP ligand decreases the potential with respect to unmodified MSN. However, DETATMS ligand substantially increases the charge of the system (Fig. 7), obtaining similar potential in materials with ligands synthesized by the two methods (43.8 ± 4.2 mV for MSN-MP-DETATMS and 41.2 ± 3.2 mV for MSN-MP+DETATMS).

In this context, the incorporation of the Sn compound does not produce a notable variation in the charge, while the functionalization with both the MP and the titanocene derivative shifts the charge of the nanostructured system to negative values due to the mercaptopropyl ligand and the metal complex (−34.3 ± 9.3 mV for MSN-MP and −20.0 ± 8.4 mV for MSN-Ti). In general, the incorporation of transferrin

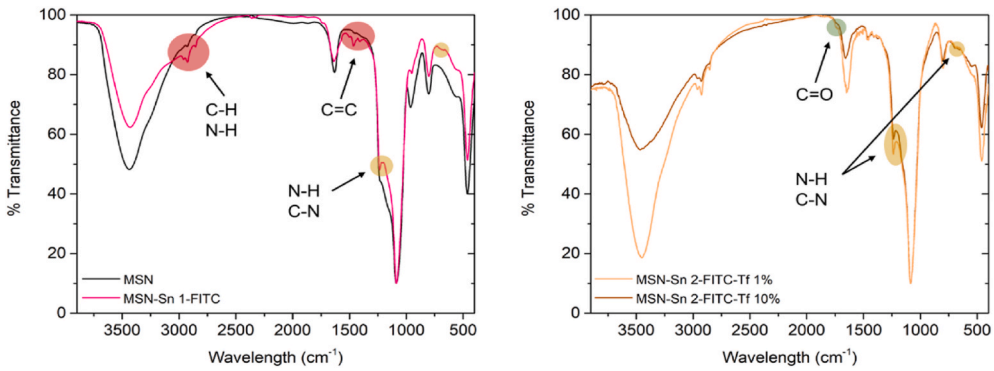

Fig. 4. FT-IR spectra of the starting material MSN and selected functionalized materials.

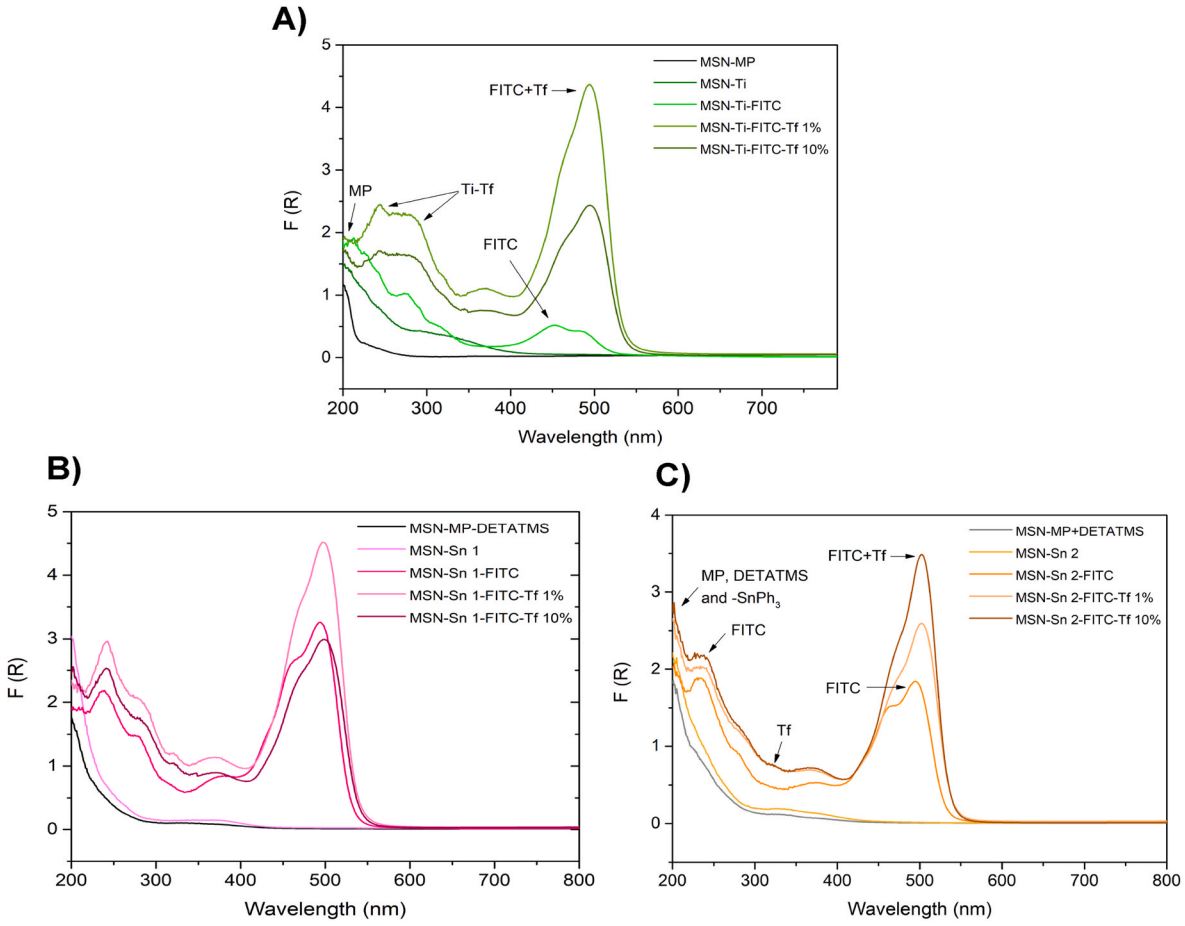

Fig. 5. Diffuse reflectance UV/Vis solid absorption spectra of titanium series (A), tin series 1 (B) and tin series 2 (C).

decreases the potential of the materials but without a significant difference between 1 and 10% of Tf. This is in agreement with that found in other nanostructured systems functionalized or coated with transferrin [39,40].

3.1.9. *Electronic microscopy studies*

Finally, the materials were characterized by SEM and TEM. The morphology and size of the functionalized nanoparticles was analysed using the ImageJ® program [41]. The TEM study (Fig. 8) shows they have a quasi-spherical morphology with a hexagonal and ordered pore distribution. The TEM images show the internal distribution of the pores, and clearly the parallel channels running through the entire mesoporous particle. The particle size distribution of the starting material was also determined observing that the parent MSNs have a particle size of 163 ± 25 nm (Fig. 8), while the final material, for example MSN-Sn 1-FITC-Tf 10%, has a particle size of 159 ± 27 nm (Figure S7). This indicates that there is no apparent influence on the morphology of the nanoparticles with the functionalization processes (Figure S8).

The analysis of the system by SEM shows the three-dimensional spherical morphology of the MSN material and its homogeneous distribution (Fig. 9 and Figure S9). In addition, one can easily observe the porosity of the material and how all the morphological characteristics are maintained in the functionalized materials (Fig. 9 and Figure S9). This indicates a good stability of the material allowing several chemical modifications without significant changes in the shape and size of the

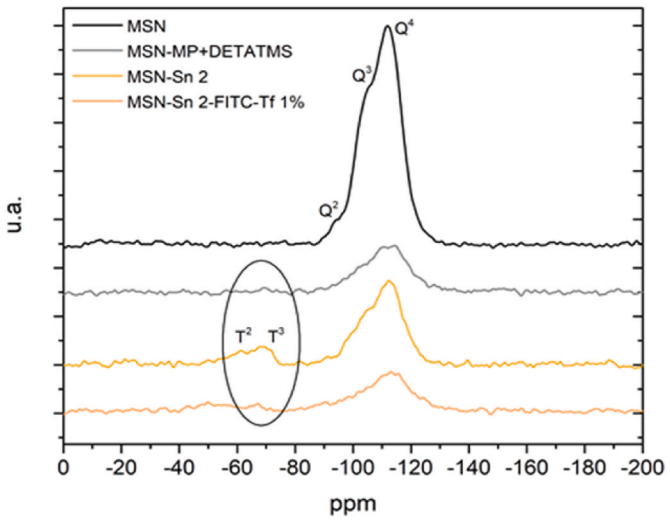

Fig. 6. ^{29}Si NMR of the materials of tin series 2.

Table 5
Electric charge (Z potential) of the MSN-based materials.

Material	Z-potential (mV)
MSN	−25.9 ± 3.9
MSN-MP	−34.3 ± 9.3
MSN-MP-DETATMS	43.8 ± 4.2
MSN-MP+DETATMS	41.2 ± 3.2
MSN-Sn 1	41.6 ± 7.4
MSN-Sn 2	36.8 ± 17.3
MSN-Ti	−20.0 ± 8.4
MSN-Sn 1-FITC	36.4 ± 13.1
MSN-Sn 2-FITC	32.3 ± 11.5
MSN-Ti-FITC	0.1 ± 12.9
MSN-Sn 1-FITC-Tf 1%	31.3 ± 15.4
MSN-Sn 1-FITC-Tf 10%	29.2 ± 8.0
MSN-Sn 2-FITC-Tf 1%	26.2 ± 8.0
MSN-Sn 2-FITC-Tf 10%	36.8 ± 8.1
MSN-Ti-FITC-Tf 1%	−36.7 ± 13.0
MSN-Ti-FITC-Tf 10%	−32.2 ± 12.8

functionalized systems. An energy-dispersive spectrometry system (EDS) was used in order to qualitatively analyze the composition of the material MSN-Sn 2-FITC-Tf 10% and confirm the presence of Sn in the system (Figure S10).

3.2. Biological studies

3.2.1. Cytotoxicity

The cytotoxicity of all materials against the A2780 ovarian cancer cell line (which overexpresses transferrin receptors) was determined. The IC_{50} values for all series of materials were obtained and compared with that of carboplatin as the reference drug (Table 6). Although the IC_{50} values of the studied materials are higher than that of carboplatin, the IC_{50} values in quantity of metal showed lower values for the MSN-based materials than for carboplatin. The most cytotoxic systems are MSN-Sn 1 and MSN-Sn 2, while when including transferrin, the materials are, unexpectedly, less cytotoxic than those without transferrin. When comparing the two different series, the tin 2 series is more cytotoxic, namely, MSN-Sn 2-FITC-Tf 1% and MSN-Sn 2-FITC-Tf 10% are more cytotoxic than MSN-Sn 1-FITC-Tf 1% and MSN-Sn 1-FITC-Tf 10%. The differences in the cytotoxicity with the varying quantities of transferrin are not significant, indicating that the amount of the transport protein does not play a crucial role in the cytotoxic activity.

Interestingly, in titanium compounds, the transferrin-functionalized material, especially with the 10% (MSN-Ti-FITC-Tf 10%) increases the cytotoxicity of the system compared with the nanomaterial without Tf (MSN-Ti). This is probably due to the fact that, as discussed previously in section 3.1.6, titanium(IV) forms a strong interaction with transferrin, which most likely facilitates the entry of the functionalized nanoparticles into the cells and subsequently promotes the release of the titanium compound in the endosomal area. This can occur via transferrin-receptor mediated route [35], thus improving the cytotoxic properties against A2780.

The functionalized MSN nanostructures displayed growth inhibitory potential against the ovarian tumour cell line A2780 in a dose-dependent manner, and their IC_{50} values are closely related to the electrokinetic Z-potential (significant negative correlation, Pearson r value −0.700, p value 0.043), indicating that the compounds which form stable colloids in the aqueous cell media usually display notable cytotoxicity.

3.2.2. Modulation of molecules from the angiogenesis signaling pathways and influence on transcription factor NF-κβ

ELISA tests were carried out to study growth factors involved in angiogenesis. VEGF-A graphic (Fig. 10A) shows that all the materials that contain a cytotoxic agent (tin or titanium) and transferrin, have less concentration of growth factor in comparison with the untreated cells, MSN and the materials only functionalized with MP and DETATMS. MSN-Sn 1 and the analogous systems with 1 and 10% of Tf showed the most significant results with lower VEGF-A concentration even than carboplatin.

The compounds were able to modulate, *in vitro*, the cellular VEGF-A and FGF-2 secretion (Fig. 10B), having implication in the new blood vessels formation in tumours (angiogenesis) and they showed interferences in signal transcription through NF-κβ activation or inhibition (Fig. 11), which is a principal regulator of progression and chemoresistance in ovarian cancer [42]. NF-κB activation in ovarian cancer cells promotes cell proliferation and metastasis, therefore NF-κB became an attractive target for drug development.

The tendency to augment or reduce the concentration of FGF-2 proteins was related to the IC_{50} values (Pearson r = −0.498, p = 0.041) but VEGF-A and NF-κβ were independent of IC_{50}, and no correlation was found among the three proteins level. Therefore, Principal Component Analysis (PCA) was performed to compare the data series in order to expose the magnitude of the compounds activity on angiogenic and apopototic pathways according to their cytotoxicity, cellular uptake and the Z-potential (a measure of the nanostructure colloidal stability).

In ovarian tumour development, the vascular endothelial growth factor (VEGF) plays a critical role in the formation of vessels, therefore, it is a suitable target for the drug candidate's inhibitory activity [43]. The role of VEGF is even more complex when the tumour cells are exposed to a metal-based drug, since VEGF has a role in the regulatory processes of metal dynamics in redox processes and the crosstalk between the tumour and the cells of the immune system, such as macrophages and lymphocytes [44]. Another pro-angiogenic factor is the basic fibroblast growth factor FGF-2, which would be expected to protect the cells survival upon the treatment with metal-based drugs. On the contrary, studies revealed that FGF-2 sensitize the A2780 cells to make them more sensitive to platinum drugs [45].

In the series of MSN materials loaded with organotin and titanocene, the best VEGF-A downregulation was observed in 3-D surface plots (Fig. 12A) in the region where FGF-2 values are relatively high, and the NF-κβ activation was not prominent (no significant activation or inhibition), corresponding to most of the MSN-Sn 1 compounds and carboplatin. FGF-2 showed an ambivalent pattern (Fig. 12B), the FGF-2/VEGF-A interdependence being fluctuant, but most elevated where NF-κβ was strongly activated, namely, in precursor MSN materials and titanocene-derivatized materials, both groups with low cytotoxicity due to the dual anti-apoptotic (through NF-κβ) versus anti-angiogenic (through VEGF-A) effects.

Clinical studies demonstrated that the clinical efficacy of carboplatin

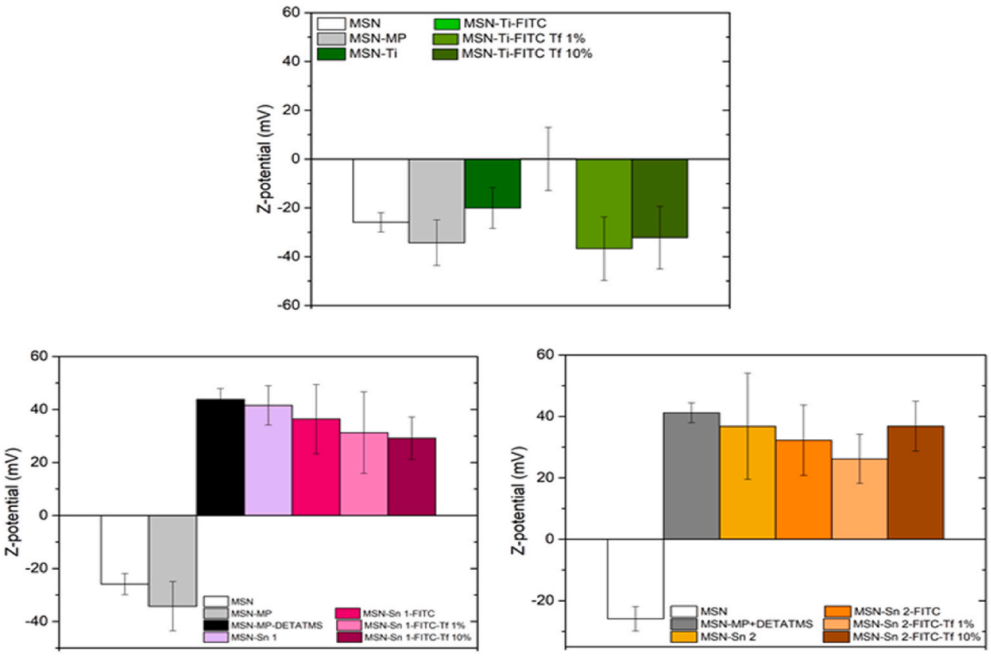

Fig. 7. Representation of Z-potential measurements of all the studied MSN materials.

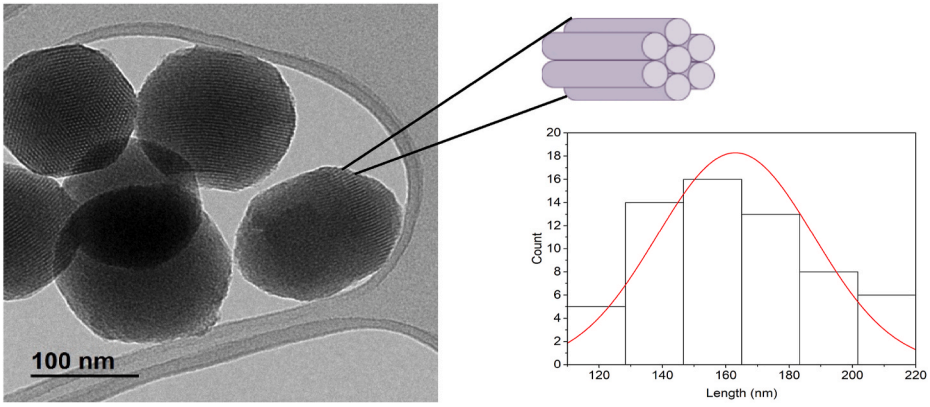

Fig. 8. TEM micrograph of MSN and its corresponding histogram.

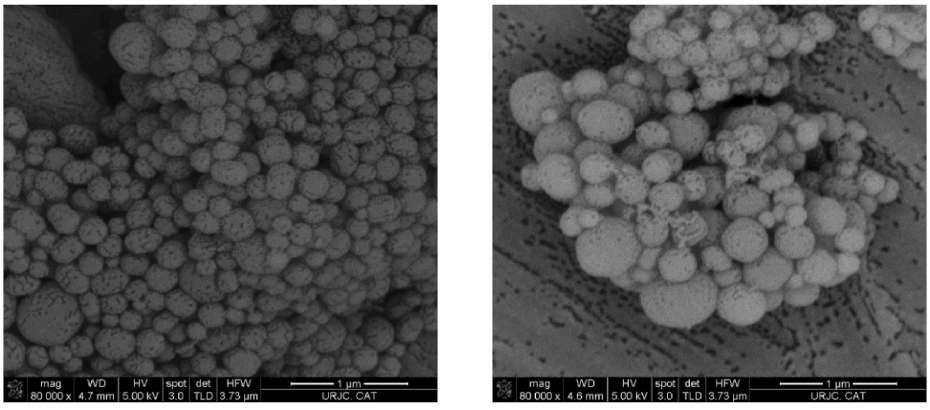

Fig. 9. SEM micrographs of MSN (left) and the final material MSN-Sn 2-FITC-Tf 10% (right).

treatment depends on NF-κβ pathway downregulation [46], while platinum-based drugs including carboplatin can induce NF-κβ suppression in epithelial tumour cells directing them towards apoptosis [47]. Similar to carboplatin, the present study showed that, generally, the precursor materials upregulate NF-κβ activation and the functionalized materials downregulate it. The compounds with just 1% Tf were capable

Table 6
Cytotoxic activity of all the materials and its reference as a function of metal content.

MATERIAL	IC_{50} (μg/mL)	IC_{50} (μg/mL) [M]
MSN	271.50 ± 8.82	–
Carboplatin	11.38 ± 0.66	5.98 ± 0.35
MSN-MP-DETATMS	112.28 ± 8.97	–
MSN-Sn 1	23.36 ± 2.16	1.04 ± 0.01
MSN-Sn 1-FITC	41.79 ± 3.75	1.87 ± 0.17
MSN-Sn 1-FITC-Tf 1%	122.30 ± 10.49	5.47 ± 0.47
MSN-Sn 1-FITC-Tf 10%	117.93 ± 7.25	5.27 ± 0.32
MSN-MP+DETATMS	125.67 ± 11.80	–
MSN-Sn 2	25.70 ± 4.25	0.12 ± 0.02
MSN-Sn 2-FITC	51.41 ± 1.76	0.25 ± 0.01
MSN-Sn 2-FITC-Tf 1%	91.19 ± 7.23	0.44 ± 0.03
MSN-Sn 2-FITC-Tf 10%	83.79 ± 3.79	0.40 ± 0.02
MSN-MP	243.97 ± 26.71	–
MSN-Ti	168.17 ± 12.21	0.76 ± 0.05
MSN-Ti-FITC	182.67 ± 18.58	0.83 ± 0.08
MSN-Ti-FITC-Tf 1%	173.20 ± 3.90	0.78 ± 0.02
MSN-Ti-FITC-Tf 10%	116.90 ± 11.40	0.53 ± 0.05

to downregulate NF-κβ stronger than their 10% Tf-functionalized analogues in the less cytotoxic MSN-Sn 1 and MSN-Ti series. The activated NF-κβ levels in these two cases were similar to that of carboplatin *in vitro*, therefore, this functionalization points towards a better *in vivo* activity. The tridimensional surface plots showed that the maximal inhibition of NF-κβ was in balance with the high FGF-2 and VEGF-A levels (Fig. 13).

The highest inhibition of soluble VEGF-A is triggered by the materials having low Z potential (see Table 5) and low IC_{50} values (an important cytotoxicity as shown in Table 5), namely, the transferrin-functionalized Sn-loaded and Ti-loaded nanostructures (Figure S11A). The inhibition of FGF-2 is not rigorously dependent either on cytotoxicity, or on Z potential (Figure S11B). The highest FGF-2 inhibition is shown in cases where the IC_{50} values are quite high (MSN-Sn 1, MSN-Sn 1-Tf) and the Z potential is high, therefore, the colloidal stability of compound in the cell suspension was also high.

The NF-κβ modulation showed a complex pattern (Figure S11C), which is not dependent on the lowest IC_{50} values, being activated by the materials with the average (MSN-Sn 1 series) or even poor cytotoxicity (MSN-Ti materials) in the studied group. NF-κβ seems to be more dependent on a high Z potential, which denotes a better stability of the cell suspension-nanomaterial system. In contrast, an activation peak is present in the absence of the compound stability or cytotoxicity, indicating that the NF-κβ activation was not the only pathway which led to cell death.

There were several convergences between the different features of the biologic activity of the novel MSN materials against A2780 cells *in vitro*, and the present study is in concordance with previous data on transferrin-functionalized nanoparticles considering the tumour microenvironment modulation and the interferences in cellular signaling [48, 49]. Previously, functionalized mesoporous nanostructures were recognized as VEGF-A [50] or FGF-2 carriers [51] and in few cases, on other cancer types, it was proven the VEGF-inhibitory effect of these materials, even without being filled with VEGF protein [52].

3.2.3. Cellular uptake assay

To determine the cellular internalization, a cellular uptake study was carried out taking benefit of the incorporation of the FITC in the materials. This study was performed in order to determine the effect of the directing agent to reach the cellular interior and it was carried out on the basis of the fluorescence intensity coming from the FITC attached to the materials.

The study was conducted using from 15 min to 4 h incubation time with the same treated cell population. It was generally observed that the maximum of fluorescence intensity was achieved after 30 min, decreasing between 2 and 4 h and then remaining stable (Fig. 14). The compound that provides the greatest cellular accumulation is that of Ti,

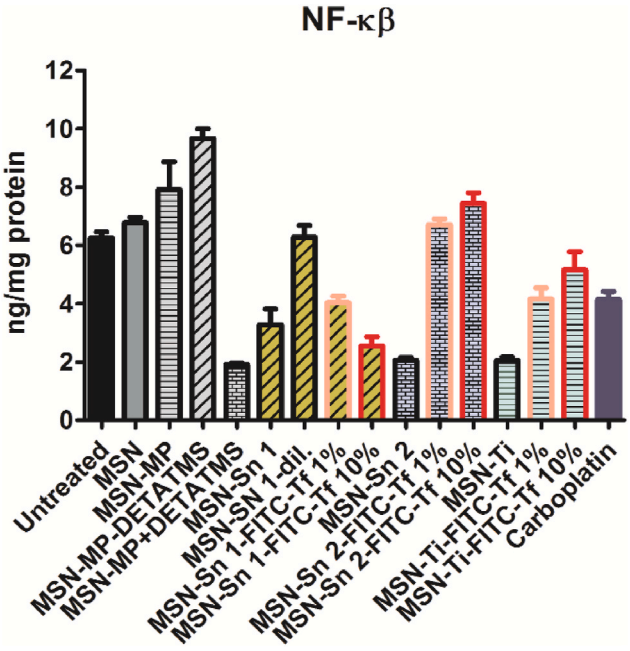

Fig. 11. The influence of functionalized MSN nanomaterials treatment on the NF-κβ transcription factor activation in A2780 cells.

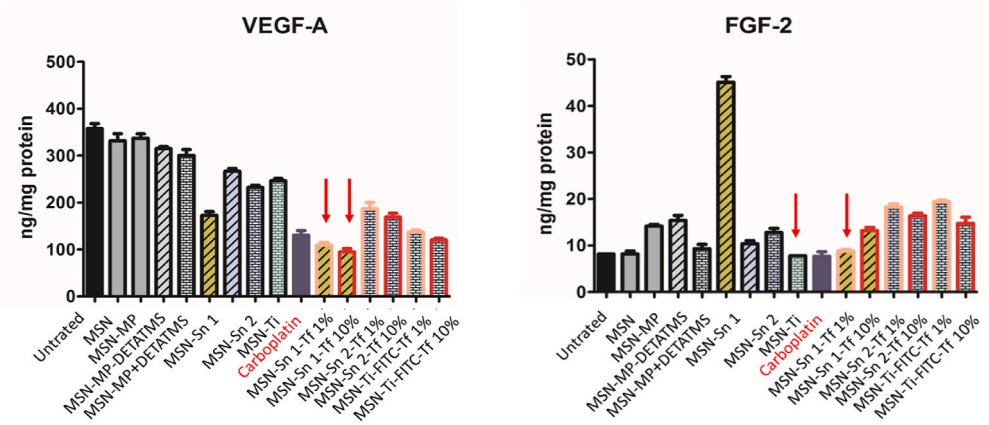

Fig. 10. The modulation of soluble VEGF-A and FGF-2 proteins secretion following the cells 24-h exposure to the nanostructures.

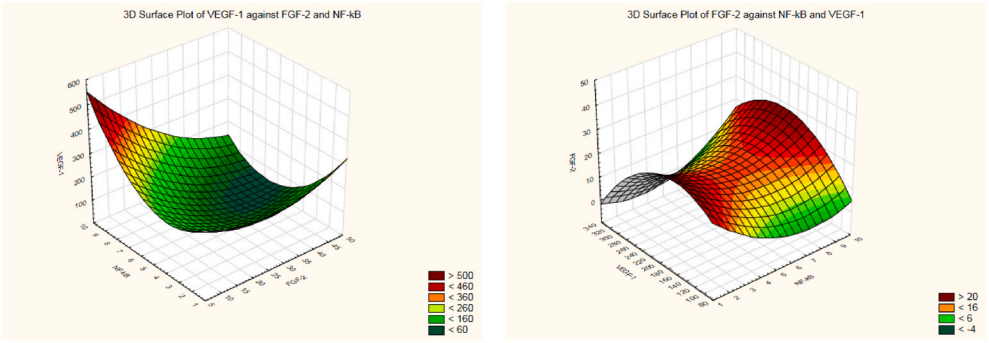

Fig. 12. PCA analysis in tridimensional quadratic surface plots of the growth factors VEGF-1 and FGF-2 and the transcription factor NF-κβ.

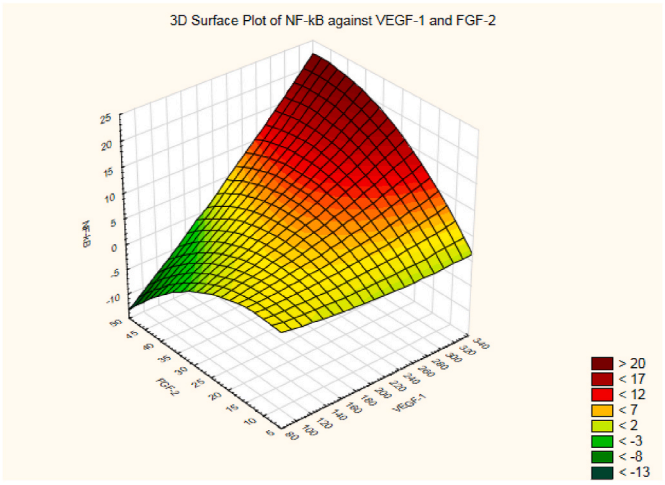

Fig. 13. Interdependence between intracellular NF-κβ activation and extracellular VEGF-A and FGF-2, as depicted in tridimensional quadratic surface plots.

although despite this, it is not the most cytotoxic material, as expected since the tin series are usually much more cytotoxic with lower doses. As for the compounds with Tf, in all cases, the incorporation is greater when there is 1% of Tf, which indicates that a higher amount of Tf is not necessary for a higher cell uptake, since with 1% percentage there is already good cellular incorporation. The interesting results in this test reinforce the idea that there is a good interaction Ti-Tf and an effective action of the protein as a Ti-transport vehicle into the cells.

The materials' cellular uptake was perfectly correlated (Pearson correlation) with the IC_{50} values in all intermediate points ($p = 0.037$ after 15 min, $p = 0.027$ at 30 min, $p = 0.033$ at 60 min, $p = 0.002$ at 120 min and $p = 0.008$ at 240 min), emphasizing the intracellular accumulation of MSN systems as a basis of cytotoxicity. In a similar way, the cellular uptake was associated with the Z potential at different exposure times when the uptake was measured ($p = 0.043$ for 15 min, $p = 0.038$ for 30 min, $p = 0.029$ for 60 min, $p = 0.005$ for 120 min and $p = 0.011$ for 240 min exposure). Therefore, the higher cytotoxic nature of the metal-functionalized MSN materials (in this case MSN-Sn 2 materials) is associated with its stability in solution and low tendency to form precipitates in the cell culture media.

3.2.4. *Stability study*

To determine the stability of the systems under physiologic conditions, a release study has been carried out in order to determine both the potential release of metal compound and/or transferrin over short time periods and also to determine if the configuration of transferrin is retained in the conjugations.

The stability study was carried out by an incubation of the materials at a physiologic pH of 7.4 in phosphate buffer at 37 °C over different time periods, quantifying the released transferrin by UV–visible spectroscopy. The results show that, in times up to 240 min the quantity of transferrin released is very low, always less than 0.1 mg/mL which corresponds to not more than 10% of the loaded Tf for those materials functionalized with 10% transferrin (See Figure S12 of Supplementary Material). In addition, an ICP analysis of the solution after the release experiments, showed no detectable metal-containing species, which confirmed the stability of the supported metallodrug and the potential action as non-classical drug delivery system [8].

Furthermore, a study of the stability of transferrin was carried out by circular dichroism (CD) spectroscopy in order gain more insight into the configuration of Tf before and after conjugation with the studied materials. In a first step, a curve evolution was measured for pure Tf at different concentrations (1.0, 0.5 and 0.1 mg/mL) in PBS buffer. The shape of alpha helix secondary structure configuration was constant, but the minimum and maximum peaks were slightly displaced (see Figure S13 of supplementary material). In this context, CD spectra of MSN-Sn2-Tf 10% and MSN-Ti-Tf 10%, filtered and unfiltered release supernatant, were

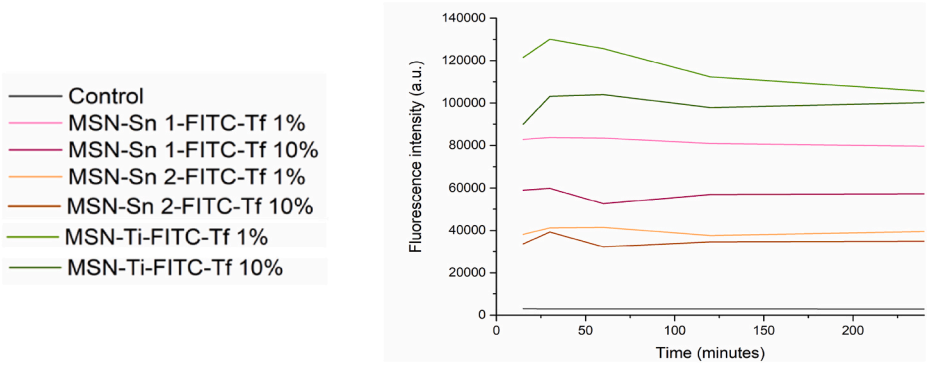

Fig. 14. Cellular uptake into the A2780 ovarian carcinoma cells *in vitro* measured at different times up to 240 min.

recorded. In the case of MSN-Sn2-Tf 10%, the alpha helix secondary structure was clearly observed for the filtered solution, while the unfiltered sample this was not as sharp although it also exhibited the same secondary conformation (Figure S14 of supplementary material). Finally, in MSN-Ti-Tf 10% material, both systems filtered and unfiltered, present identical low intensity CD curves, indicating a more intense interaction between Ti and Tf compared to that observed for the MSN-Sn2-Tf 10% system, resulting in a lower release of transferrin. However, in both cases the alpha helix shape can also be observed (See Figure S15 of supplementary material) indicating that the structural conformation of Tf remains unchanged after conjugation, although the release proportion is lower for Ti-based material MSN-Ti-Tf 10% compared with MSN-Sn2-Tf 10%, supporting the premise of a stronger interaction for Ti-Tf than for Sn-Tf. In addition, in both titanium and tin systems, stability of the transferrin configuration has been observed.

4. Conclusions

In this study, different functionalized mesoporous silica-based systems containing cytotoxic agents based on Sn and Ti have been prepared with the ligands MP and DETATMS. Furthermore, FITC was incorporated as a fluorophore for the analysis of cellular internalization of materials. Transferrin, as a target agent of cell line A2780, was also incorporated in the nanomaterials. The incorporation of transferrin at 1 or 10% in weight in the materials of the tin series was carried out through the primary amines of the DETATMS ligand via an EDAC-mediated coupling reaction, while for the titanium material the transferrin seems to be incorporated directly interacting with the organometallic derivative most likely due to the strong Ti-Tf interaction. In general, the IC_{50} values of all the materials, expressed as a function of the functionalized metal quantity, shows a higher cytotoxic activity than carboplatin (in some cases even up to 50 times higher), indicating the promising potential of the systems in anticancer chemotherapy. However, the differences in the interaction of the materials with transferrin led to different behaviours of the final materials in their cellular internalization, observing a greater accumulation inside the cell of the titanium-functionalized systems, with just 1% of Tf being sufficient for a rapid accumulation in cells as early as in the first 15 min of incubation. The role of transferrin is to assist in the internalization of all the functionalized silica-based nanoparticles, in spite of what was observed in other studies with Tf-liposomes [53], in which the internalization is reduced because of the interaction with some other proteins. Nevertheless, the incorporation of transferrin in the silica-based materials studied here does not lead to significant improvements in the cytotoxic activity compared to materials without this protein or when using different transferrin quantities.

The study of growth factors VEGF-A, FGF-2 and NF-κβ transcription factor showed that the MSN materials were able to modulate and down-regulate these factors highlighting the Sn systems. We demonstrated, in ovarian cancer cell populations, that the Sn or Ti functionalized mesoporous nanomaterials, even without being loaded with growth factors, show anti-angiogenic effects through VEGF-A and FGF-2 modulation showing different behaviour in Sn- and Ti-containing materials co-functionalized with transferrin, since this protein, a Fe carrier, is usually strongly involved in angiogenesis [54].

In summary, for the first time in the literature a new series of multifunctional-MSN materials with therapeutic fragments based on Sn and Ti compounds, an imaging agent such as FITC and formulated in transferrin have been synthesized and characterized and have demonstrated encouraging cytotoxic potential and internalization (dependent on transferrin) in ovarian cancer A2780. These materials represent a promising advance for future studies in this field, which will be focused on the combination of the internalization potential of Ti-Tf-functionalized systems with the highly cytotoxic nature of Sn-functionalized compounds in a single platform.

Acknowledgement

We would like to thank the funding of the Ministerio de Ciencia e Innovación of Spain (former Ministerio de Ciencia Innovación y Universidades of Spain), grant number RTI2018-094322-B-I00. The biologic part of this work was supported by a grant of Ministry of Research and Innovation, CNCS-UEFISCDI, project number PN–III–P4-ID-PCCF-2016-0142, within PNCDI III. Universidad Rey Juan Carlos (International School of Doctorate) and Banco de Santander are gratefully acknowledged for the mobility scholarship for D. D.-G. to obtain International Doctor mention.

CRediT authorship contribution statement

Diana Díaz-García: Conceptualization, Methodology, Investigation, Visualization, Writing – original draft, Writing – review & editing. **Eva Fischer-Fodor:** Conceptualization, Methodology, Resources, Investigation, Supervision, Writing – original draft, Writing – review & editing. **Cătălin Ioan Vlad:** Methodology, Resources, Investigation. **José M. Méndez-Arriaga:** Methodology, Investigation. **Sanjiv Prashar:** Methodology, Supervision, Investigation, Writing – review & editing. **Santiago Gómez-Ruiz:** Conceptualization, Methodology, Resources, Supervision, Writing – original draft, Writing – review & editing, All the authors have supervised and agreed with the final version of this manuscript.

Declaration of competing interest

The authors declare that they have no known competing financial interests or personal relationships that could have appeared to influence the work reported in this paper.

Appendix A. Supplementary data

Supplementary data to this article can be found online at https://doi.org/10.1016/j.micromeso.2021.111238.

References

[1] S. Roy, C.K. Ghosh, C.K. Sarkar, Nanotechnology: Synthesis to Applications, CRC Press, 2018. https://www.crcpress.com/Nanotechnology-Synthesis-to-Applications/Roy-Ghosh-Sarkar/p/book/9781138032736.
[2] N. Iturrioz-Rodriguez, M.A. Correa-Duarte, M.L. Fanarraga, Controlled drug delivery systems for cancer based on mesoporous silica nanoparticles, Int. J. Nanomed. 14 (2019) 3389–3401, https://doi.org/10.2147/IJN.S198848.
[3] K.H. Bae, H.J. Chung, T.G. Park, Nanomaterials for cancer therapy and imaging, Mol. Cell 31 (2011) 295–302, https://doi.org/10.1007/s10059-011-0051-5.
[4] A. Rai, S. Noor, S.I. Ahmad, M.F. Alajmi, A. Hussain, H. Abbas, G.M. Hasan, Recent advances and implication of bioengineered nanomaterials in cancer theranostics, Medicina 57 (2021) 91, https://doi.org/10.3390/medicina57020091.
[5] A. Baeza, M. Vallet-Regí, Mesoporous silica nanoparticles as theranostic antitumoral nanomedicines, Pharmaceutics 12 (2020) 957, https://doi.org/10.3390/pharmaceutics12100957.
[6] A. Dasgupta, I. Biancacci, F. Kiessling, T. Lammers, Imaging-assisted anticancer nanotherapy, Theranostics 10 (2020) 956–967, https://doi.org/10.7150/thno.38288.
[7] C. Monneret, Platinum anticancer drugs. From serendipity to rational design, Ann. Pharm. Fr. 69 (2011) 286–295, https://doi.org/10.1016/j.pharma.2011.10.001.
[8] W.A. Wani, S. Prashar, S. Shreaz, S. Gómez-Ruiz, Nanostructured materials functionalized with metal complexes: in search of alternatives for administering anticancer metallodrugs, Coord. Chem. Rev. 312 (2016) 67–98, https://doi.org/10.1016/j.ccr.2016.01.001.
[9] J.A. Benjamín-Rivera, A.E. Cardona-Rivera, Á.L. Vázquez-Maldonado, C.Y. Dones-Lassalle, H.L. Pabón-Colon, H.M. Rodríguez-Rivera, I. Rodríguez, J.C. González-Espiet, J. Pazol, J.D. Pérez-Ríos, J.F. Catala-Torres, M. Carrasquillo Rivera, M.G. De Jesus-Soto, N.A. Cordero-Virella, P.M. Cruz-Maldonado, P. González-Pagan, R. Hernández-Ríos, K. Gaur, S.A. Loza-Rosas, A.D. Tinoco, Exploring serum transferrin regulation of nonferric metal therapeutic function and toxicity, Inorganics 8 (2020) 48, https://doi.org/10.3390/inorganics8090048.
[10] J.B. Vincent, S. Love, The binding and transport of alternative metals by transferrin, Biochim. Biophys. Acta 1820 (2012) 362–378, https://doi.org/10.1016/j.bbagen.2011.07.003.
[11] K. Ishiwata, T. Ido, M. Monma, M. Murakami, H. Fukuda, M. Kameyama, K. Yamada, S. Endo, S. Yoshioka, T. Sato, T. Matsuzawa, Potential

radiopharmaceuticals labeled with titanium-45, Int. J. Radiat. Appl. Instrum. Appl. Radiat. Isot. 42 (1991) 707–712, https://doi.org/10.1016/0883-2889(91)90173-X.
[12] H. Sun, H. Li, R.A. Weir, P.J. Sadler, The first specific TiIV -protein complex: potential relevance to anticancer activity of titanocenes, Angew Chem. Int. Ed. Engl. 37 (1998) 1577–1579, https://doi.org/10.1002/(SICI)1521-3773(19980619)37:11<1577::AID-ANIE1577>3.0.CO;2-M.
[13] P.T. Gomme, K.B. McCann, J. Bertolini, Transferrin: structure, function and potential therapeutic actions, Drug Discov. Today 10 (2005) 267–273, https://doi.org/10.1016/S1359-6446(04)03333-1.
[14] M. Koc, S. Taysi, O. Sezen, N. Bakan, Levels of some acute-phase proteins in the serum of patients with cancer during radiotherapy, Biol. Pharm. Bull. 26 (2003) 1494–1497, https://doi.org/10.1248/bpb.26.1494.
[15] H. Li, Z.M. Qian, Transferrin/transferrin receptor-mediated drug delivery, Med. Res. Rev. 22 (2002) 225–250, https://doi.org/10.1002/med.10008.
[16] A. Jhaveri, P. Deshpande, B. Pattni, V. Torchilin, Transferrin-targeted, resveratrol-loaded liposomes for the treatment of glioblastoma, J. Contr. Release 277 (2018) 89–101.
[17] L. Rocamora-Reverte, E. Carrasco-García, J. Ceballos-Torres, S. Prashar, G. N. Kaluđerović, J.A. Ferragut, S. Gómez-Ruiz, Study of the anticancer properties of tin(IV) carboxylate complexes on a panel of human tumor cell lines, ChemMedChem 7 (2012) 301–310, https://doi.org/10.1002/cmdc.201100432.
[18] J. Ceballos-Torres, P. Virag, M. Cenariu, S. Prashar, M. Fajardo, E. Fischer-Fodor, S. Gómez-Ruiz, Anti-cancer applications of titanocene-functionalised nanostructured systems: an insight into cell death mechanisms, Chem. Eur J. 20 (2014) 10811–10828, https://doi.org/10.1002/chem.201400300.
[19] C. Bensing, M. Mojić, S. Gómez-Ruiz, S. Carralero, B. Dojčinović, D. Maksimović-Ivanić, S. Mijatović, G.N. Kaluđerović, Evaluation of functionalized mesoporous silica SBA-15 as a carrier system for $Ph_3Sn(CH_2)_3OH$ against the A2780 ovarian carcinoma cell line, Dalton Trans. 45 (2016), https://doi.org/10.1039/c6dt03519a, 18984–18993.
[20] Y. Ellahioui, S. Prashar, S. Gómez-Ruiz, Anticancer applications and recent investigations of metallodrugs based on gallium, tin and titanium, Inorganics 5 (2017) 4, https://doi.org/10.3390/inorganics5010004.
[21] S. Gómez-Ruiz, A. García-Peñas, S. Prashar, A. Rodríguez-Diéguez, E. Fischer-Fodor, Anticancer applications of nanostructured silica-based materials functionalized with titanocene derivatives: induction of cell death mechanism through TNFR1 modulation, Materials 11 (2018), https://doi.org/10.3390/ma11020224.
[22] D. Díaz-García, D. Cenariu, Y. Pérez, P. Cruz, I. del Hierro, S. Prashar, E. Fischer-Fodor, S. Gómez-Ruiz, Modulation of the mechanism of apoptosis in cancer cell lines by treatment with silica-based nanostructured materials functionalized with different metallodrugs, Dalton Trans. 47 (2018) 12284–12299, https://doi.org/10.1039/C8DT01677A.
[23] D. Díaz-García, L. Sommerova, A. Martisova, H. Skoupilova, S. Prashar, T. Vaculovic, V. Kanicky, I. del Hierro, R. Hrstka, S. Gómez-Ruiz, Mesoporous silica nanoparticles functionalized with a dialkoxide diorganotin(IV) compound: in search of more selective systems against cancer cells, Microporous Mesoporous Mater. (2020), 110154, https://doi.org/10.1016/j.micromeso.2020.110154.
[24] D. Díaz-García, K. Montalbán-Hernández, I. Mena-Palomo, P. Achimas-Cadariu, A. Rodríguez-Diéguez, E. López-Collazo, S. Prashar, K. Ovejero Paredes, M. Filice, E. Fischer-Fodor, S. Gómez-Ruiz, Role of folic acid in the therapeutic action of nanostructured porous silica functionalized with organotin(IV) compounds against different cancer cell lines, Pharmaceutics 12 (2020) 512, https://doi.org/10.3390/pharmaceutics12060512.
[25] K. Ovejero Paredes, D. Díaz-García, V. García-Almodóvar, L. Lozano Chamizo, M. Marciello, M. Díaz-Sánchez, S. Prashar, S. Gómez-Ruiz, M. Filice, Multifunctional silica-based nanoparticles with controlled release of organotin metallodrug for targeted theranosis of breast cancer, Cancers 12 (2020) 187, https://doi.org/10.3390/cancers12010187.
[26] Y. Zhao, B.G. Trewyn, I.I. Slowing, V.S.-Y. Lin, Mesoporous silica nanoparticle-based double drug delivery system for glucose-responsive controlled release of insulin and cyclic AMP, J. Am. Chem. Soc. 131 (2009) 8398–8400, https://doi.org/10.1021/ja901831u.
[27] A.D. Andreicuț, E. Fischer-Fodor, A.E. Pârvu, A.B. Țigu, M. Cenariu, M. Pârvu, F. A. Cătoi, A. Irimie, Antitumoral and Immunomodulatory Effect of Mahonia Aquifolium Extracts, Oxidative Medicine and Cellular Longevity, 2019, e6439021, https://doi.org/10.1155/2019/6439021.
[28] M. Thommes, K. Kaneko, A.V. Neimark, J.P. Olivier, F. Rodriguez-Reinoso, J. Rouquerol, K.S.W. Sing, Physisorption of gases, with special reference to the evaluation of surface area and pore size distribution (IUPAC Technical Report), Pure Appl. Chem. 87 (2015) 1051–1069, https://doi.org/10.1515/pac-2014-1117.
[29] N.X. Dat Mai, U.-C. Nguyen Le, L.H. Thuy Nguyen, H.T. Kieu Ta, H. Van Nguyen, T. M. Le, T.B. Phan, L.-T. Thi Nguyen, F. Tamanoi, T. Le Hoang Doan, Facile synthesis of biodegradable mesoporous functionalized-organosilica nanoparticles for enhancing the anti-cancer efficiency of cordycepin, Microporous Mesoporous Mater. 315 (2021), 110913, https://doi.org/10.1016/j.micromeso.2021.110913.
[30] S.K. Nethi, N.A.A. P, B. Rico-Oller, A. Rodríguez-Diéguez, S. Gómez-Ruiz, C. R. Patra, Design, synthesis and characterization of doped-titanium oxide nanomaterials with environmental and angiogenic applications, Sci. Total Environ. (2017) 1263–1274, https://doi.org/10.1016/j.scitotenv.2017.05.005.
[31] J. Karges, D. Díaz-García, S. Prashar, S. Gómez-Ruiz, G. Gasser, Ru(II) polypyridine complex-functionalized mesoporous silica nanoparticles as photosensitizers for cancer targeted photodynamic therapy, ACS Appl. Bio Mater 4 (2021) 4394–4405, https://doi.org/10.1021/acsabm.1c00151.
[32] V.A. Lorenz-Fonfria, Infrared difference spectroscopy of proteins: from bands to bonds, Chem. Rev. 120 (2020) 3466–3576, https://doi.org/10.1021/acs.chemrev.9b00449.
[33] I. del Hierro, S. Gómez-Ruiz, Y. Pérez, P. Cruz, S. Prashar, M. Fajardo, Mesoporous SBA-15 modified with titanocene complexes and ionic liquids: interactions with DNA and other molecules of biological interest studied by solid state electrochemical techniques, Dalton Trans. 47 (2018) 12914–12932, https://doi.org/10.1039/C8DT02011F.
[34] I. del Hierro, Y. Pérez, P. Cruz, R. Juárez, Pt and Ti complexes immobilized onto mesoporous silica microspheres and their interaction with molecules of biological interest, Eur. J. Inorg. Chem. 2017 (2017) 3030–3039, https://doi.org/10.1002/ejic.201700235.
[35] M. Guo, H. Sun, H.J. McArdle, L. Gambling, P.J. Sadler, Ti(IV) uptake and release by human serum transferrin and recognition of Ti(IV)-transferrin by cancer cells: understanding the mechanism of action of the anticancer drug titanocene dichloride, Biochemistry 39 (2000) 10023–10033, https://doi.org/10.1021/bi000798z.
[36] V.S. Bollu, A.K. Barui, S.K. Mondal, S. Prashar, M. Fajardo, D. Briones, A. Rodríguez-Diéguez, C.R. Patra, S. Gómez-Ruiz, Curcumin-loaded silica-based mesoporous materials: synthesis, characterization and cytotoxic properties against cancer cells, Mater. Sci. Eng. C Mater. Biol. Appl. 63 (2016) 393–410, https://doi.org/10.1016/j.msec.2016.03.011.
[37] R. Kotcherlakota, A.K. Barui, S. Prashar, M. Fajardo, D. Briones, A. Rodríguez-Diéguez, C.R. Patra, S. Gómez-Ruiz, Curcumin loaded mesoporous silica: an effective drug delivery system for cancer treatment, Biomater. Sci. 4 (2016) 448–459, https://doi.org/10.1039/C5BM00552C.
[38] D. Pérez-Quintanilla, A. Sánchez, I. del Hierro, M. Fajardo, I. Sierra, Synthesis and characterization of novel mesoporous silicas of the MSU-X family for environmental applications, J. Nanosci. Nanotechnol. 9 (2009) 4901–4909, https://doi.org/10.1166/jnn.2009.1106.
[39] S. Sheykhzadeh, M. Luo, B. Peng, J. White, Y. Abdalla, T. Tang, E. Mäkilä, N. H. Voelcker, W.Y. Tong, Transferrin-targeted porous silicon nanoparticles reduce glioblastoma cell migration across tight extracellular space, Sci. Rep. 10 (2020) 2320, https://doi.org/10.1038/s41598-020-59146-5.
[40] G. Aragoneses-Cazorla, J. Serrano-Lopez, I. Martinez-Alfonzo, M. Vallet-Regí, B. González, J.L. Luque-Garcia, A novel hemocompatible core@shell nanosystem for selective targeting and apoptosis induction in cancer cells, Inorg. Chem. Front. (2021), https://doi.org/10.1039/D1QI00143D.
[41] ImageJ, National Institutes of Health, USA. https://imagej.nih.gov/ij/. (Accessed 21 February 2021).
[42] B.S. Harrington, C.M. Annunziata, NF-κB signaling in ovarian cancer, Cancers 11 (2019) 1182, https://doi.org/10.3390/cancers11081182.
[43] Y. Chen, L. Zhang, W. Liu, K. Wang, VEGF and SEMA4D have synergistic effects on the promotion of angiogenesis in epithelial ovarian cancer, Cell. Mol. Biol. Lett. 23 (2018) 2, https://doi.org/10.1186/s11658-017-0058-9.
[44] M. Serra, A. Columbano, U. Ammarah, M. Mazzone, A. Menga, Understanding metal dynamics between cancer cells and macrophages: competition or synergism? Front. Oncol. 10 (2020) https://doi.org/10.3389/fonc.2020.00646.
[45] A.B. Coleman, M.Z. Metz, C.A. Donohue, R.E. Schwarz, S.E. Kane, Chemosensitization by fibroblast growth factor-2 is not dependent upon proliferation, S-phase accumulation, or p53 status, Biochem. Pharmacol. 64 (2002) 1111–1123, https://doi.org/10.1016/s0006-2952(02)01268-6.
[46] P.A. Konstantinopoulos, E. Fountzilas, K. Pillay, L.F. Zerbini, T.A. Libermann, S. A. Cannistra, D. Spentzos, Carboplatin-induced gene expression changes in vitroare prognostic of survival in epithelial ovarian cancer, BMC Med. Genom. 1 (2008) 59, https://doi.org/10.1186/1755-8794-1-59.
[47] Y. Shen, J. Wang, T. Yang, Y. Li, W. Jiang, Z. Guan, Z. Wang, J. Tan, J. Wu, G. Li, Q. Xu, F. Wu, L. Wang, Y. Liu, Platinums sensitize human epithelial tumor cells to lymphotoxin α by inhibiting NF-κB-dependent transcription, Canc. Biol. Ther. 7 (2008) 1407–1414, https://doi.org/10.4161/cbt.7.9.6429.
[48] J. Fu, W. Li, X. Xin, D. Chen, H. Hu, Transferrin-Modified nanoliposome codelivery strategies for enhancing the cancer therapy, J. Pharmaceut. Sci. 109 (2020) 2426–2436, https://doi.org/10.1016/j.xphs.2019.11.013.
[49] M. Bouchoucha, É. Béliveau, F. Kleitz, F. Calon, M.-A. Fortin, Antibody-conjugated mesoporous silica nanoparticles for brain microvessel endothelial cell targeting, J. Mater. Chem. B. 5 (2017) 7721–7735, https://doi.org/10.1039/C7TB01385J.
[50] Y. Chen, X. Wang, T. Liu, D.S.-Z. Zhang, Y. Wang, H. Gu, W. Di, Highly effective antiangiogenesis via magnetic mesoporous silica-based siRNA vehicle targeting the VEGF gene for orthotopic ovarian cancer therapy, Int. J. Nanomed. 10 (2015) 2579–2594, https://doi.org/10.2147/IJN.S78774.
[51] X. Wang, Q. Liu, W. Chen, L. Liu, FGF adsorbed mesoporous bioactive glass with larger pores in enhancing bone tissue engineering, J. Mater. Sci. Mater. Med. 30 (2019) 48, https://doi.org/10.1007/s10856-019-6252-8.
[52] M. Zhang, L. Jiang, Doxorubicin hydrochloride-loaded mesoporous silica nanoparticles inhibit non-small cell lung cancer metastasis by suppressing VEGF-mediated angiogenesis, J. Biomed. Nanotechnol. 12 (2016), https://doi.org/10.1166/jbn.2016.2290.
[53] A. Salvati, A.S. Pitek, M.P. Monopoli, K. Prapainop, F.B. Bombelli, D.R. Hristov, P. M. Kelly, C. Åberg, E. Mahon, K.A. Dawson, Transferrin-functionalized nanoparticles lose their targeting capabilities when a biomolecule corona adsorbs on the surface, Nat. Nanotechnol. 8 (2013) 137–143, https://doi.org/10.1038/nnano.2012.237.
[54] X. Li, G.-F. Fu, Y.-R. Fan, C.-F. Shi, X.-J. Liu, G.-X. Xu, J.-J. Wang, Potent inhibition of angiogenesis and liver tumor growth by administration of an aerosol containing a transferrin-liposome-endostatin complex, World J. Gastroenterol. 9 (2003) 262–266, https://doi.org/10.3748/wjg.v9.i2.262.